Paleo-environment and provenance in a lacustrineshallow-water delta - meandering river sedimentary system: Insights from the Middle-Upper Jurassic formations of the Fukang Sag of Junggar Basin, NW China.

Long Luo[a,b,c], Xianzhi Gao[a,b]*, Xianfeng Tan[d], Jon Gluyas[c], Jinduo Wang[e], Xiangye Kong[f], Jinzhao Huang[g], Hengbo Shao[a] , Futao Qu[a]

[a] College of Geosciences, China University of Petroleum, Beijing 102249, China

[b] State Key Laboratory of Petroleum Resources and Prospecting (China University of Petroleum, Beijing), Beijing102249, China

[c] Department of Earth Sciences, Durham University, Durham, DH1 3LE, UK

[d] Chongqing Key Laboratory of Complex Oil and Gas Field Exploration and Development, Chongqing University of Science and Technology, Chongqing 401331, China.

[e] Exploration and Development research institution, Shengli Oilfield Branch Company of Sinopec

[f] Unconventional Natural Gas Institute, China University of Petroleum, Beijing, 102249, China

[g] Second oil production plant of Changqing Oilfield Company, China National Petroleum Corporation, Qingyang 744100, China.

*Corresponding authors: College of Geosciences, China University of Petroleum (Beijing), 18 Fuxue Road, Changping District, Beijing 102249, China.

*E-mail addresses: gaoxz1963@163.com (X. Gao), longluo988@163.com (L. Luo),

Abstract

The Middle-Upper Jurassic Shishugou Group in the central Junggar Basin was deposited in a lacustrine -shallow water delta-meandering river sedimentary system. The integrated petrological (thin-section, granularity and heavy minerals analysis), geochemical (trace elements and rare earth elements analysis) and geophysical analyses (well logging and 3D-seismic slice analysis) are intended to revealthe redox conditions,

palaeo-climate, palaeo-salinity, provenance and sedimentary evolution extant during deposition of the Shishugou Group and determine the relationships among them: the redox condition changed from a weak anoxic/oxic condition to a strongly oxic condition; the climate changed from humid to hot and arid in the Middle-Late Jurassic, which may have resulted in the lake water having slight – medium salinity; the relatively distant northeastern provenance from Kelameili Mountain is the most important sediment source, and the south provenance from the Tianshan Mountains (Bogeda Shan) decreases with the development of the Sag piedmont, which only supplies sediments for the southeastern Fukang Sag. The sedimentary environment changed from a lake - shallow water delta to a meandering river during the deposition of the Shishugou Group. The shallow-water meandering river delta was characterized by pervasive mudstones with oxide colours, thin single-layer sand bodies (1-15 m, av.3m), relatively low sand-strata ratios (0.2-0.5) and the lack of progradation, mouth bar and reverse rhythm.The gentle slope is the primary condition necessary for the formation of a shallow-water meandering river delta. Palaeo-environment (climate change from Warm-humid to hot-arid) and stable and far Kelameili Mountain provenance played critical roles in the development and evolution of lacustrine- delta-meandering river sedimentary systems.

Keywords

Palaeoclimate; Redox condition; Palaeosalinity; Warm humid; Hot arid; Shishugou Group; Fukang Sag

1. Introduction

The provenance, palaeo-environment including palaeoclimate, redox conditions and palaeo-salinity are important factors used to decipher the sedimentary distribution and evolution and are key in revealing the relationship among the palaeo-environment, provenance and evolution of the depositional system (Lv et al., 2016; Potter-Mclntyre

et al., 2016, Lv et al., 2017). The climate, which may determine the lake level, redox condition and salinity, is one of most important environmental controls on sedimentary characteristics (Engelmann et al., 2004; Jone et al., 2014; Lv et al., 2014; Kim et al., 2015; Lv et al., 2017; Liu et al., 2018). The concept of shallow-water delta was proposed in 1954 (Fisk et al.,1954). The lacustrine shallow-water delta is generally formed in comprehensive conditions including shallow water depth (less than several tens of meters), gentle slope, lake level change and stable provenance.Besides, it is characterized by hot-arid climate, pervasive red mudstone, fine-grained sandstone, thin single sand-body and low ratio of sandstone in strata (Lemons and Chen,1999; Zhu et al.,2012; Zhu et a.,2013; Zhu et al.,2016).

The Jurassic was a typical greenhouse period and was predominantly characterized by global warmth and atmospheric CO_2 levels as much as four times as large as the present (Berner and Geocarb, 1994; Huber et al., 2000; Sellwood and Valdes, 2008). Hence, the Jurassic palaeoclimate has been one of the popular topics of sedimentary environment research (Moore et al., 1992; Berner and Geocarb, 1994; Huber et al., 2000; Sellwood and Valdes, 2008; Myers et al., 2011; Galloway et al., 2013; Wierzbowski et al., 2013; Souto and Fernandes, 2017; El-Sabbagh et al., 2017; Martínez-Yanez et al., 2017). There were five stages of palaeoclimatic evolution in China, and the palaeoclimate regionalization was different during these stages (Deng et al., 2017). The Jurassic formations of the Junggar Basin of northwestern China are currently important hydrocarbon exploration targets, especially the Fukang Sag, which is located in the centre of the Junggar Basin. Moreover, the sedimentary characteristics of Middle-Upper Jurassic formations have remarkable variability, perhaps due to the palaeoclimate conditions and provenance. However, few publications referencing the Jurassic palaeoclimate of the Junggar Basin of China exist (Deng et al., 2017; Zhu et al., 2017).

77 The provenance of the Jurassic Shishugou Group is almost universally accepted in the
78 eastern Fukang slope of central Junggar basin, but thereis some controversy in the
79 central and eastern Fukang Sag (e.g. the fourth region of Central Junggar basin) (Zhang
80 et al.,1999;Shang et al.,2011; Ji et al.,2014;Su et al.,2014).

81 The primary objective of this study is to determine the provenance of the clastic
82 rock and the palaeoenvironmental conditions present during the Middle-late Jurassic
83 period in the Junggar Basin. This study also aims to reveal the relationship between the
84 palaeo-environment, provenance and lake-shallow water delta- meandering river
85 sedimentary system.

86 **2. Geological setting**

87 The Junggar Basin is located in Xinjiang Uygur Autonomous Region , northwestern China. The subtriangular basin is surrounded by six mountains formed by belts of thrust faults (Fig. 1). The northwestern boundary is defined by Zaire Mountain and Halahaalate Mountain; the northeastern boundary is defined by Qinggelidi Mountain and Kelameili Mountain; and the southern boundary is defined by the North Tianshan, including Eren Habirga Mountain and Bogeda Mountain (Fig. 1)（Luo et al.,2018; Wang et al.,2018）. The Fukang Sag, which is located close to the central Junggar Basin, is a piedmont Sag of North Tianshan (Fig. 1).

95 The initial uplift of the southern part of Bogeda Mountain occurred in the early-
96 middle Jurassic（Greene, 2001； Gong et al., 2015）. The rapid uplift of both southern
97 Bogda Mountain and northeastern Kelameili Mountain occurred in the early Jurassic
98 but slowed in the middle Jurassic. The uplift of Bogda Mountain was clearly faster than
99 that of northeastern Kelameili Mountain during the deposition of the Shishugou Group
100 (Gong et al., 2015）. Consequently, the Fukang Sag now slopes gently to the southwest
101 (Luo et al., 2018).

The formations that comprise the Jurassic stratum include the Badaowan (J_1b), Sangonghe (J_1s), Xishanyao (J_2x), Toutunhe (J_2t) and Qigu (J_3q) Formations (Fig. 2). The regional angular unconformity on the top of the Qigu Formation (Fig. 2) was formed by the tectonic uplift of the Junggar Basin (Wu, 1986; Li et al., 2006). Qigu Formation has been strongly eroded because of the unconformity, so the remaining Qigu Formation is thin and difficult to be identified accurately. Moreover, both Toutunhe and Qigu Formation are very important to the research of paleo-environment and sedimentary evolution. Therefore, we usually research them together as the Shishugou Group. The Middle-late Jurassic Shishugou Group comprising Toutunhe and Qigu Formations were buried to a depth of 3600-5800 m, deposited in a lacustrine-deltaic-meandering fluvial sedimentary system in the Fukang Sag (Zhu et al., 2017). The Toutunhe Formation consists of the first member (J_2t^1), the second member (J_2t^2) and the third member (J_2t^3). The lacustrine basin depth clearly decreased during the deposition of the Shishugou Group, meanwhile, the palaeoclimate became clearly hot and dry (Fig. 2) (Zhu et al., 2017).

According to high-resolution sequence stratigraphy (Cross, 1994), the Shishugou Group in the Junggar Basin exhibits two long-term stratigraphic base-level circles (3rd-order sequences), as shown in Fig. 2. The Toutunhe Formation can be divided into one long-term stratigraphic base-level cycle (LSC), and subdivided into three middle base-level cycles (MSC1, MSC2, MSC3) and ten short cycles (SSC1-SSC10) (Fig. 2). The Qigu Formation, which consists of one LSC, can be divided into three middle base-level cycles (MSC1, MSC2, MSC3) and subdivided into at most eight short cycles (SSC1-SSC8) (Fig. 2) (Zhang et al., 2000; Wang et al., 2001; Yu et al., 2014; Yu et al., 2016). The Qigu Formation is generally composed of less than eight SSC due to the erosion represented by the upper unconformity (Fig. 2).

3. Materials and methods

Datasets used in this investigation consist of seismic slices, well logs, conventional cores and outcrop sections. The three-dimensional seismic data consists of three parts and covers most of the Fukang Sag. The seismic slices with amplitude attributes are chopped nearly along the layer or target formation. Fifty-six representative core samples were collected from the Toutunhe and Qigu Formations, from 8 wells and 10 outcrop samples from the field section in the Fukang Sag. Thirty-two thin sections, which were impregnated with blue epoxy resin, were used for petrological and mineralogical analyses by 300-point counts. The granularity analysis was performed on 28 sandstone samples by measuring 400 grains per thin section under a microscope.

The original geochemical signatures of mudstone can remain relatively well-preserved during deposition due to its grain size and impermeability (McCulloch and Wasserburg, 1978; Sochava et al., 1994; Cullers, 1995; Graver and Scott, 1995). The current geochemical characteristics of a mudstone include trace elements and rare earth elements, which are deposited in sedimentary basins without significant fractionation, generally preserving the original signature of the source materials (Floyd et al., 1990). Therefore, the current geochemical characteristics of mudstones are widely used in provenance studies of clastic rocks (Dickinson and Suczek, 1979; Bhatia, 1983; McLennan et al., 1983; Bhatia and Crook, 1986; Roser and Korsch, 1986; McLennan and Taylor, 1991; Owen et al., 1999;). In addition, some trace elements (e.g., Sr, Cu, and Rb) in the mudstone, which are sensitive to palaeoenvironmental parameters, are generally used to decipher the palaeotectonic setting and the palaeoclimate conditions (Worash, 2002; Zhang et al., 2006; Zhao et al., 2007; Cao et al., 2012). Eleven mudstone samples were collected from cores of the 7 wells; 6 of the samples come from the J_3q, and 5 come from the J_2t. The trace elements and Rare Earth Elements (REE) of 11

mudstone samples were analysed using ICP-MS (DRC-e). Repeated analysis of USGS reference materials OU-6, AMH-1 and GBPG-1 shows that the analytical precision of most trace elements was better than 95%.

In addition, most heavy minerals are derived from specific source rocks and controlled by their provenance; therefore, heavy mineral analysis is the most common techniques for provenance determination (Morton and Hallsworth, 1999; Svendsen and Hartley, 2002; Mange and Wright, 2007; Garzanti et al., 2008; Morton et al., 2011; Nieet al., 2012; Sevastjanova et al., 2012; Do Nascimento Jr et al., 2015; Bassis et al., 2016; Aubrecht et al., 2017). The heavy mineral composition of a source rock can be altered and modified by many processes such as chemical weathering, hydraulic sorting during transport, sorting by grain size, diagenetic alteration during deposition and burial processes (Morton and Hallsworth, 1999; Garzanti et al.,2008, 2009). Therefore, some heavy mineral (HM) assemblages, which are sensitive to their environment, can also be used to evaluate the approximate palaeogeographic conditions, including palaeoclimate, palaeo-environment and palaeotopography (Parfenoff et al., 1970; Mange and Maurer, 1992; Dill, 1998; Jin et al., 2002; Dinis and Soares, 2007; Lin et al., 2008; Liu, 2012). Heavy minerals analysis was performed on 30 samples, which were collected from the Toutunhe and Qigu Formations, to identify the species, characteristics and contents of the heavy minerals. Moreover, the heavy mineral data of 56 samples in East Fukang slope were collected from Xinjiang Oil field and previous published results (Ji et al.,2014).

4. Results

4.1 Petrology of sandstones

The Shishugou Group sandstones in the Fukang Sag are predominantly litharenite, according to Folk's (1980) sandstone classification scheme, averaged as $Q_{43.8}F_{7.4}R_{48.8}$

177 (Luo et al. 2018). Lithic grains (R) are the most common detrital component,
178 representing approximately 48.8% (average value) of the detrital grain volume and
179 consisting of volcanic, metamorphic and minor sedimentary rock fragments (Fig. 3a-f)
180 (Luo et al., 2018). The detrital grains, which are characterized by poor to moderate
181 sorting, are mostly fine-grained but also contain a small number of silty and medium-
182 sized grains (Fig. 3). The rock fragments of the J_2t conglomerate sampled from outcrop
183 consist of volcanic and metamorphic rock fragments (Fig. 3g-i). The rock fragments of
184 the J_3q medium sandstone from outcrop mostly comprise metamorphic rock fragments,
185 with a minor constituent of volcanic rock fragments (Fig. 3g-i).

186 4.2 Heavy minerals of sandstone

187 The heavy mineral assemblages mainly comprise epidote (relative content: 0% to
188 84.7%, av. 32.4%), limonite (relative content: 0%-81.7%; av. 23.8%), garnet (relative
189 content: 0%-25.9%, av. 4.6%), zircon (relative content: 0%-21.1%, av. 3.5%), barite
190 (relative content: 0%-76.9%, av. 12.1%), magnetite (0%-16.9%, av. 3.2%) and pyrite
191 (relative content: 0%-99.1%, av. 8.3%) (Table 1). Pyrite occasionally occurs at the strata
192 of certain wells, such as the D1, D7 and D11 wells, and is mainly observed in the first
193 (J_2t^1) and second (J_2t^2) sub-member of the Toutunhe Formation sandstones (Table 1,
194 Fig. 4, Fig. 5). The abundance of limonite increases as the age of the sandstones
195 decreases (Fig. 6, Fig. 7). The relative limonite content of the first sub-member of the
196 Toutunhe Formation (J_2t^1) sandstones ranges from 0.0% to 1.8% (av. 0.3%); the
197 limonite content of the second sub-member (J_2t^2) sandstones varies from 0.0% to 81.7%
198 (av. 29.3%); the limonite content of the third sub-member (J_2t^3) sandstones varies from
199 0.2% to 61.2% (av. 31.1%); and the limonite content of the Qigu Formation (J_3q)
200 sandstones varies from 20.2% to 67% (av. 50.5%)(Table 1).

201 The ZTR values of Shishugou Group sandstones vary from 0.1 to 66.4 (with an

202 average value of 9.7). The Qigu Formation (J_3q) sandstones have ZTR values ranging
203 from 1.7 to 16.5 (av. 7.0) (Table 1). The ZTR values of the Toutunhe Formation
204 sandstones varies from 0.1 to 66.4 (with an average value of 10.0); the first sub-member
205 of Toutunhe Formation (J_2t^1) sandstones have ZTR values ranging from 0.1 to 66.4 (av.
206 17.2); the ZTR values of the second sub-member (J_2t^2) sandstones vary from 0.4 to 28.5
207 (with an average value of 8.0); and the ZTR values of the third sub-member (J_2t^3)
208 sandstones vary from 0.2 to 9.9 (with an average value of 3.2) (Table 1).

209 4.3 Trace element geochemistry of mudstone

210 The abundance of 33 trace elements in the mudstones has been measured to
211 reconstruct the palaeoenvironment. Representative ratios (Rb/Sr, Sr/Cu, Sr/Ba, U/Th
212 and V/Cr) can help to unravel the palaeoenvironment (palaeoclimate, palaeosalinity and
213 redox conditions) (Epstein and Mayeda, 1953; Lerman and Gat, 1989; Zheng and Liu.,
214 1999; Jin and Zhang, 2002; Meng et al., 2012; Bai et al., 2015; Moradi et al., 2016; Cao
215 et al., 2015; Moradi et al., 2016). The Sr/Ba ratio varies from 0.34 to 0.62 with an
216 average value of 0.48. The U/Th ratio varies from 0.10 to 0.48 with an average value
217 of 0.26. The Sr/Cu ratio varies from 1.38 to 16.19 with an average value of 6.82. The
218 V/Cr ratio varies from 0.43 to 2.59 with an average value of 1.30 (Table 2). The vertical
219 profiles of the redox-sensitive elements measured (Cd, U, Ta and Mo) and their related
220 ratios (Rb/Sr, Sr/Cu, Sr/Ba, U/Th and V/Cr) in the mudstones are illustrated in Fig. 8.
221 Raw data are provided in Table 2.

222 4.4 REE geochemistry of mudstone

223 The total Rare Earth Element (REE) concentrations in the Shishugou Group
224 mudstone varies from 146.47 ppm to 1413.04 ppm (with an average value of 442.61
225 ppm) (Table 3). The shale-normalised (NASC) REE concentration is characterized by
226 an essentially flat pattern, with La_N/Yb_N values varying from 0.8 to 1.35 (av. 1.06)

(Table 3, Fig. 9). In addition, they have a relative enrichment of light REE (LREE), with Ce_N/Yb_N values ranging from 0.94 to 16.97 (av. 4.79) (Table 3, Fig. 9). The REE concentrations of three samples (D8-6, D3-7, D6-6) markedly peak at Ce, with an additional peak at Er (Table 3, Fig. 9).

Most REE, especially Ce, Er and Gd, have relatively high concentrations in the middle-upper part of J_2t^2 and the middle-lower part of the J_2t^3 and relatively low concentrations in the other parts of the Shishugou Group (Fig. 10). The microfacies of all samples from J_2t^2 and D6-6 from J_3q mainly include subaqueous interdistributary bay and subaqueous natural levee.

The relative enrichment or depletion in Ce relative to La and Pr is expressed as the Ce anomaly and is quantified as the ratio $Ce/Ce^* = (Ce_N)/(La_N + Pr_N) \times 0.5$, where N represents the shale-normalized (NASC) values (Murray et al. 1992). The Eu anomaly was calculated by $Eu/Eu^* = Eu_N/(Sm_N + Gd_N) \times 0.5$ (Murray et al., 1992; Owen et al., 1999). The Ce/Ce* values are almost all less than 1, representing a negative anomaly, but three samples (such as D8-6, D3-7, and D6-6) are greater than 1, representing a positive anomaly (Table 3). The Eu/Eu* values of all samples are less than 1, which represents a negative anomaly. La_N/Yb_N values vary from 0.8 to 1.35 with an average value of 1.06 (Table 3).

4.5 Sedimentary facies

4.5.1 Facies association A (Shore-shallow lacustrine facies)

4.5.1.1 Description

The lithofacies of facies association A is composed of grey-dark grey mudstone, siltstone and fine sandstone (Fig. 11). The lithofacies associations were characterized by sandstone/mudstone couplets that form a rhythmically interbedded succession at several metres to ten metres in scale (Fig. 11). The sedimentary structures included

252 wave ripples, current bedding, lenticular bedding, and cross bedding. Carbon fragments
253 were distributed along the bedding plane (Fig. 11). In the cumulative curve of particle
254 size, the probability of bar and beach sandstone consist of three sections, in which the
255 bouncing-dominated component consists of two sections (Fig. 11). The well log gamma
256 (GR) curve shows finger-, serrated- and funnel-shaped low amplitude variations (Fig.
257 11).

258 4.5.1.2 Interpretation

259 The carbon fragments may originate from the semi-deep to deep lacustrine
260 environments. The grey-dark grey mudstones, siltstones and fine sandstones containing
261 carbon fragments were deposited in a relatively deep-water environment near a semi-
262 deep lacustrine environment. Furthermore, the interbedded relationship of the
263 mudstone and sandstone, the well-log curve (GR), the cumulative particle size
264 probability curve and the sedimentary structures present suggest that the shore-shallow
265 lacustrine facies and the beach and bar sandstones are the most important sand bodies
266 (Fig. 11). The facies association A can be interpreted as the shore-shallow lacustrine
267 facies (Fig. 11).

268 4.5.2 Facies association B (Shallow-water meandering-river delta front)

269 4.5.2.1 Description

270 Lithofacies of facies association B include green grey-grey siltstone, fine
271 sandstone (several metres to tens of metres in scale) and mudstone with a relatively low
272 sand-strata ratio (0.2 to 0.5) (Fig. 12). The sedimentary structures include parallel
273 bedding, current bedding, cross-bedding and basal erosion scouring structures, wave
274 ripples, sphenoid cross-bedding, lenticular bedding and slump structures. The
275 cumulative particle size probability curve of the main sand body, which has a relatively
276 steep slope, comprise two sections representing the more abundant bouncing

277 component and the more minor suspension-transport component (Fig. 12). The GR
278 curve of the main sand body generally shows bell-shaped or box- and funnel-shaped
279 middle amplitude variations. The GR curve of the interbedded siltstones and mudstones
280 shows serrated low-amplitude variations (Fig. 12).

281 4.5.2.2 Interpretation

282 The main green grey- grey sand body exhibiting parallel bedding, current bedding,
283 and cross-bedding was deposited in a shallow water environment and influenced by
284 wave action. The basal erosional scour structures observed also suggest that the river
285 channel was eroded. The slump structures and the cumulative particle size probability
286 curve are generally indicative of a delta front environment (Fig. 12). Therefore, the
287 main green grey-grey sand body can be interpreted as a subaqueous distributary channel
288 of the delta front. The sand body with the funnel-shaped GR curve is likely a mouth bar,
289 on the basis of characteristics of the cumulative curve (Fig. 12). The interbedded
290 siltstone and mudstone succession may be interpreted as the subaqueous natural barrier
291 of the delta front. The green grey-grey succession generally represents an
292 interdistributary bay. Consequently, the facies association B represent a shallow-water
293 meandering-river delta front (Fig. 12).

294 4.5.3 Facies association C (Shallow-water meandering-river delta plain)

295 4.5.3.1 Description

296 Lithofacies of facies association C comprise the grey-green, brown and brownish-
297 red interbedded fine-sandstones and mudstones (Fig. 13). The sand-mud ratio (0.4-0.8)
298 of the interbedded succession is lower than that of facies association B (0.8-1.2). The
299 sedimentary structures observed include parallel bedding, current bedding, low-angle
300 tabular/wedge-shaped cross-bedding and basal erosional scour structures. The
301 cumulative particle size probability curve of the main sand body that has a relatively

steep slope comprise three sections, representing the dominant bouncing transport and minor rolling and suspension transport (Fig. 13). The GR curve of the main sand body generally exhibits box-shaped middle-high amplitude variations and a bell-shape if the thickness of the sand body is relatively small. The GR curve of grey-green, brown and brownish-red interbedded siltstone and mudstone shows serrated low-amplitude variations (Fig. 13).

4.5.3.2 Interpretation

The grey-green, brown and brownish-red interbedded fine sandstone and mudstone unit that has a relatively low sand-mud ratio (0.4-0.8) is suggestive of an intermittently exposed shallow water environment. The grey-green and brown fine-sandstones with low-angle tabular/wedge-shaped cross-bedding and basal erosional scour structures indicate river channel erosion. In addition, the GR curve and the cumulative particle size probability curve of the main sand body also provide evidence for a channel branch of the delta plain (Fig. 13). Therefore, the grey-green, brown and brownish-red interbedded siltstones and mudstones can be interpreted as the natural barrier of the delta plain. The massive succession of grey-green, brown and brownish-red mudstone can be interpreted as an arid interchannel depression, which is different from a marsh (Fig. 13). Hence, facies association C should be interpreted as the shallow-water delta plain of a meandering river (Fig. 13).

4.5.4 Facies association D (Meandering river)

4.5.4.1 Description

Lithofacies of facies association D exhibit relatively low sand-mud ratios (0.2 to 0.5) and consist of brownish-red/taupe fine-medium sandstone, mudstone and some coarse sandstone (Fig. 14). The sedimentary structures observed include parallel bedding, low-angle tabular/wedge-shaped cross-bedding, and basal erosional scour

structures. The climbing-ripple bedding and current bedding can be observed in the interbedded siltstone and mudstone succession. Horizontal bedding and lenticular bedding were observed in the mudstone succession. The cumulative particle size probability curve of the main sand body that has a relatively gentle slope comprise two sections representing bouncing and suspension transport; the relatively high percentages of suspension transport vary from 20% to 50% (Fig. 14). Some coarse sandstones consist of rolling, bouncing and suspension-transport components. The well-log gamma (GR) curve of the main sand body generally shows a dentate-box or dentate-bell shape and middle-high amplitude variations (Fig. 14). The GR curve of the brownish-red/taupe interbedded siltstone and mudstone shows serrated middle-low amplitude variations (Fig. 14).

4.5.4.2 Interpretation

The brownish-red/taupe lithofacies is indicative of an exposed oxidizing environment. The main fine-medium sand body has a relatively low sand-mud ratio and is characterized by low-angle tabular/wedge-shaped cross-bedding and basal erosional scour structures, suggestive of river channel erosion. In addition, the GR curve and the cumulative particle size probability curve also suggest that the main fine-medium sand body can be interpreted as a point bar and some of the coarse sandstone can be interpreted as a channel-lag deposit. The brownish-red/taupe interbedded siltstone and mudstone with climbing ripple bedding can be interpreted as a natural barrier. The brownish-red/taupe mudstone succession represents a floodplain. As a whole, facies association D was deposited in a meandering river environment (Fig. 14).

5. Discussions

5.1 Redox condition

The redox-sensitive parameters related to the geochemistry are widely used to

352 qualitatively decipher palaeo-environment, palaeo-water depth and offshore distance
353 because deep lacustrine settings are generally anoxic and shallow lacustrine to fluvial
354 settings are mainly dysoxic to oxic (Algeo et al., 2010; Tan et al., 2017). The
355 concentration and ratio value of redox-sensitive trace elements and rare earth elements
356 are redox indicators of the palaeo-environment (Fig. 14) (Elderfield and Greaves, 1982;
357 Barwise, 1990; Jones and Manning, 1994; Betchtal et al., 2001; Adegoke et al., 2014;
358 Hu et al., 2016; Tan et al., 2017; Kuzyk et al., 2017).

359 The varying Ce^{3+} ion concentrations and redox condition are well demonstrated
360 by the Ce anomaly in both marine and lacustrine settings, so the critical parameters
361 (e.g., Ce_{anom}) related to the Ce anomaly are widely used to estimate the palaeo-redox
362 conditions (Wilde et al., 1996). A positive cerium anomaly of the samples, characterized
363 by Ce/Ce* values greater than 1, suggests low-oxygen depositional conditions.
364 Conversely, a negative cerium anomaly, characterized by Ce/Ce* values less than 1,
365 represents an oxidizing depositional environment (Murthy et al., 2004).

366 Most of the samples with negative cerium anomalies have Ce/Ce* values
367 suggestive of oxidizing conditions, but three samples (D8-6, D3-7, D6-6) with positive
368 anomalies are indicative of low-oxygen/reducing conditions (Table 3) (Murthy et al.,
369 2004). A negative Eu/Eu* (less than 1) may indicate the preferential loss of Ca-bearing
370 minerals during weathering and deposition or may reflect the sediment sources (Murthy
371 et al. 2004). The negative anomaly of Eu/Eu* values in the Shishugou Group mudstone
372 suggests oxidizing conditions (Table 3) (Sverjensky, 1984; Murthy et al., 2004).

373 The Th/U ratio was generally used to examine the redox conditions of the
374 depositional environment (Wignall and Twitchett, 1996). U is mobile under oxic
375 conditions but relatively immobile under anoxic conditions so anoxic sediments are
376 much more enriched in U than oxic sediments (Baioumy and Lehmann, 2017). Th is

stable under redox conditions and immobile in any aqueous environment. Therefore, low Th/U ratios or high U/Th ratios indicate reducing conditions. The ratio of U/Th, which ranges from 0.1 to 0.48 with an average value of 0.24, suggests that the Shishugou Group mudstones were mainly deposited in oxidizing conditions (Table 3, Fig. 8i) (Pi et al. 2014). The V/Cr ratios below 2 represent oxic depositional conditions; V/Cr ratios ranging from 2 to 4.25 suggest dysoxic conditions; and V/Cr ratios over 4.25 indicate an anoxic-suboxic environment (Jones and Manning, 1994). V/Cr values of the Shishugou Group range from 0.43 to 2.59, with an average of 1.30, and suggest that the Shishugou Group was mainly deposited in oxidizing conditions (Table 2, Fig. 8f).

The V/Ni ratio has been widely used to determine the redox condition present during deposition. V/Ni ratios higher than 3 indicate that mudstones were deposited under anoxic conditions, while V/Ni ratios varying between 1.9 and 3 indicate that mudstones were deposited in a dysoxic-oxic environment (Galarraga et al., 2008). The V/Ni ratios in the Shishugou Group mudstones, which vary between 0.81 and 3.38, with an average of 2.4, decrease as the age of the strata decreases (Table 2, Fig. 8k). Some mudstones of J_2t^1 and J_2t^2 have relatively high V/Ni ratios, higher than 3 (Table 2, Fig. 8k). These results indicate that the Shishugou Group mudstones were mainly deposited in a dysoxic-oxic environment and some mudstones of J_2t^1 and J_2t^2 may have been deposited in reducing conditions (Fig. 15, Fig. 16). Most of the Shishugou Group mudstones display V/(V + Ni) ratios below 0.8 and V/(V + Cr) ratios below 0.6, indicating the dysoxic-oxic condition present during their deposition (Tables 2, Fig. 9l-m, Fig. 15,Fig. 16) (Zhou and Jiang, 2009; Pi et al., 2014; Baioumy and Lehmann, 2017).

The occurrence of the heavy mineral pyrite generally reflects anoxic/reducing

conditions or a warm humid climate present during deposition, and limonite suggests the presence of oxidizing conditions or a hot arid climate (Jin et al., 2002; Lin et al., 2008; Liu, 2012). Pyrite, which is mainly observed in the first (J_2t^1) and second (J_2t^2) sub-members of the Toutunhe Formation sandstones in some wells (Table 1, Fig. 4, Fig. 5), suggests anoxic/reducing conditions and high lake water levels (Fig. 15, Fig. 16). The limonite content, which increases as the age of the strata decreases, is mainly found in J_2t^2, J_2t^3 and J_3q (Fig. 6, Fig. 7), indicating that the dominant oxidizing conditions become more intense as the age of strata decreases (Fig. 15,Fig. 16).

5.2 Palaeo-salinity and Palaeoclimate

Strontium (Sr) and barium (Ba) can provide evidence for palaeo-salinity because the Sr/Ba ratio generally increases as the salinity of ambient water increases (Epstein and Mayeda, 1953; Cao et al., 2015; Moradi et al., 2016; Zhang et al., 2017). The Sr/Ba ratios of the Shishugou Group samples vary from 0.34 to 0.62, with an average of 0.48, indicating that the lake was filled with slight-medium salinity water during deposition (Table 2, Fig. 8j) (Zhang et al., 2017). Furthermore, the increasing Sr/Ba ratio of the Shishugou Group suggests that the slight-medium salinity of lake water changed over time (Table 2, Fig. 8j).

The climate can influence the geochemical signatures of sediments by its controls on the exogenic processes and terrigenous sediment flux into lacustrine environments (Tanaka et al., 2007; Meng et al., 2012; Bai et al., 2015). Therefore, the geochemical signatures of samples may provide evidence of palaeoclimatic conditions present during the deposition of the sediment (Worash, 2002). The Rb/Sr and Sr/Cu ratios of sediments are important indicators of palaeoclimatic conditions (Bai et al., 2015; Moradi et al., 2016). Substantially high ratios of Rb/Sr (0.44~1.14, average 0.81) of the samples demonstrate semiarid or arid conditions during deposition of the Shishugou

427 Group (Table 2, Fig. 8h, Fig. 15, Fig. 16,Fig. 17, Fig. 18).

428 The Sr/Cu ratios that range from 1.3 to 5 represent a warm-humid climate, while
429 ratios over 5 indicate a hot-arid climate (Lerman, 1978). The Sr/Cu ratios of the
430 mudstone in J_2t range nearly from 1 to 6 (av. 4.22), indicating a warm humid-hot arid
431 climate condition (Table 2, Fig. 8i, Fig. 16, Fig. 17, Fig. 18). The Sr/Cu ratios of J_3q
432 mudstone are clearly higher than 5, which suggests a hot arid climate condition (Table
433 2, Fig. 8i, Fig. 16, Fig. 17, Fig. 18). Therefore, the change in the Sr/Cu ratio can be
434 interpreted as a change in palaeoclimate from warm-humid to hot-arid conditions (Table
435 2, Fig. 8i, Fig. 16, Fig. 17, Fig. 18). In addition, the abundance of the drought-enduring
436 Gymnospermae classopollis within the Shishugou Group also indicates that the palaeo-
437 climate was hot and arid as a whole (Fig. 18) (Zhu et al., 2017). The salinity change of
438 lake water closely corresponds to the palaeoclimate changes, because climate change
439 generally exerts a significant effect on the salinity of lake water by evaporation and
440 atmospheric rainfall (Fig. 18).

441 5.3 Provenance

442 The Shishugou Group has three main provenances, including northeastern ,eastern
443 Beisantai and southern sediment sources in the Fukang Sag (Zhang et al.,1999;Ji et al.,
444 2014; Zou et al., 2014; Gong, 2015; Zhu et al., 2017). The dominant northeastern
445 provenance from Kelameili Mountain consists of dominantly volcanic rock fragments,
446 with minor amounts of metamorphic rock fragments (Fig. 1B) (Ji et al., 2014; Zou et
447 al., 2014). Moreover, some previous researches show that both the eastern Beisantai
448 and northeastern provenances might be derived from Kelameili Mountain (Shang et
449 al.,2011; Ji et al.,2014). According to thin section analysis of rock samples from the
450 field, the southern sediment source of the Tianshan Mountains (Bogeda Shan) is
451 characterized by the dominance of metamorphic rock fragments, with minor

452 contributions of volcanic rock fragments, although volcanic rock fragments are slightly
453 more prevalent than metamorphic rock fragments in the early deposition of the
454 Toutunhe Formation (Fig. 3g-l). The lithological change from conglomerate to medium
455 sandstone in the field outcrop indicates the decreasing supply capacity of the southern
456 provenance (Fig. 3g-l).

457 The ZTR values obviously vary in different members sandstone (J_2t^1, J_2t^2, J_2t^3, J_3q)
458 of the Shishugou Group, which generally indicate some changes of provenances in
459 study area during deposition (Fig. 15). Besides, the epidote content distribution, the 3-
460 D seismic slices, ZTR and previous published result (Zhang et al.,1999) show that the
461 sediments of J_2t^1 mainly came from the northeastern and southern provenances, the J_2t^2
462 and J_2t^3 derived from northeastern, southern and eastern (Beisantai heave) provenances,
463 the J_3q derived from northeastern and eastern (Beisantai heave) sediment sources (Fig.
464 15). The supply range of southern provenance gradually decreased during deposition
465 process in the south-eastern of study area (eastern Fukang slope) (Fig. 15). The 3-D
466 seismic slices and uplift of North Santai heave demonstrate that the supply capacity of
467 eastern provenance increased during the deposition of Toutunhe Formation (Fig. 15)
468 (Zhang et al.,1999).

469 However, some research indicates that the eastern provenance (Beisantai) came
470 from the north of Beisantai but not the Beisantai heave (Shang et al.,2011). Moreover,
471 the eastern provenance (Beisantai) started to provide sediments for the Fukang Sag
472 during the deposition of J_2t^2 (Fig. 15a-b). Therefore, the mother rock of eastern
473 provenance probably came from the J_2t^1 sediments of Beisantai and Kelamei Mountain.
474 The relative abundances of the remaining heavy minerals largely unaffected by the
475 specific transport, deposition and burial processes, provided information on similar
476 hydraulic and diagenetic behaviour (Morton and Hallsworth, 1999). Epidote is not only

typically regarded as metamorphic minerals of igneous granitoid rocks but also the magmatic minerals originated from Plutons (Zen and Hammarstrom,1984), so the relative content of epidote provided important information about the provenance of the sediments. The heavy minerals of Shishugou Group sandstones, which mainly comprise the epidote, limonite and barite, indicate that the mother rock types of provenance were relatively simple and related with volcanic rocks and metamorphic rocks. Rare earth elements (REEs) are significant indicators of provenance because they are not extensively redistributed during transport, deposition and post-depositional processes (Nelson and DePaolo, 1988; McLennan, 1989; Liu et al., 2018). The almost-flat REE patterns with La_N/Yb_N values varying from 0.8 to 1.35 and averaging 1.06 indicate that the sediment source of the Shishugou Group is almost entirely from the same provenance (Table 3) (Fig. 9). Few samples show an obvious enrichment of Ce, which may be related to the partial redox conditions (Fig. 9). These indicate that the mother rocks of both northeastern and eastern (Beisantai heave) provenance came from the Kelameili Mountain and the southern provenance was very limited in the fourth region of central Junggar basin.

The petrology, heavy mineral distribution, 3-D seismic slices and geological setting suggest that the Kelameili Mountain provenance including northeastern and eastern provenances, influenced the greatest range of the sediments in the Fukang Sag, and the southern provenance, the Tianshan Mountains (Bogeda Shan), supplied sediments for only a very limited area of the southeastern Fukang Sag (Fig. 3a-i, Fig. 15 a-d). The supply area of the southern provenance decreased as the piedmont Sag developed, generated by the fast uplift of Bogda Shan during the deposition of Shishugou Group (Fig. 15a-d). Uplift of North Santai heave and south steep slope generated by fast uplift of Bogda Shan restricted the supply range of south provenance,

especially in the fourth region of central Junggar Basin (Shang et al., 2011; Gong,2015), which can be explained by the alluvial fans of Toutunhe Formation in front of the Bogda Mountain (Fig. 3g). The rate and degree of chemical weathering on continents are mainly controlled by moisture and temperature conditions related to the climate, so a warm and humid climate may favour chemical weathering (Nesbitt and Young, 1982; Yan et al., 2007). The climate change from humid to hot and arid conditions may reduce the weathering rates and supply capacity of sediment provenance (Fig. 18) (Algeo and Twitchett, 2010; Liu et al., 2018).

5.4 Characteristics and evolution of sedimentary facies

The progradation, mouth bar and reverse rhythm，which are typical characteristics of the normal delta, were rarely observed in the shallow-water meandering river delta (Fig. 12, Fig. 13; Fig. 15, Fig. 16). The sandstone mainly consists of siltstone and fine sandstone (Fig. 11, Fig. 12, Fig. 13, Fig. 14). The green-grey, brown and brownish-red mudstone were pervasive in the shallow-water meandering river delta facies (Fig. 11, Fig. 12, Fig. 13, Fig. 14, Fig. 16).Obviously, the granularity size of sandstone of shallow-water meandering river delta is generally less than normal delta, but the oxide colours of mudstone are very pervasive in the shallow-water delta. The sedimentary structures include parallel bedding, current bedding, cross-bedding and basal erosional scour structures in the shallow-water delta. The shallow-water meandering river delta sedimentary succession has a large overall thickness but relatively thin single-layer sand bodies (1-15 m, av.3m) and relatively low sand-strata ratios (0.2-0.55), which are obviously less than that of the normal delta (Fig. 11, Fig. 12, Fig. 13, Fig. 14). The meandering river facies are characterized by the thin, fine-medium grained point bar sandstones and a lack of marsh deposits (Fig. 15, Fig. 16, Fig. 17).

During deposition of J_2t^1, the sedimentary environment consisted of lake and

shallow-water meandering river delta front. The sedimentary facies of J_2t^1 are characterized by the "big front-small plain" delta (BFBPD), which dominantly comprise the shallow-water meandering river delta front with minor constituents of a shallow-water meandering river delta plain (Fig. 15a, Fig. 16a, Fig. 17a, Fig. 18). The plain range of J_2t^2 increased in comparison with the J_2t^1 (Fig. 15b, Fig. 16b). Conversely, the depositional facies of J_2t^3 is the "big plain-small front" delta (BPBFD), which dominantly consists of a shallow-water meandering river delta plain environment with minor shallow-water meandering river delta front constituents (Fig. 15c, Fig. 16c, Fig. 17b, Fig. 18). Therefore, the shallow-water meandering river delta plain environment rapidly transformed into a meandering river environment during the deposition of J_3q (Fig. 15d, Fig. 16d, Fig. 17c, Fig. 18).

5.5 The relationships among palaeo-environment, provenance and sedimentary systems

The gentle slope structure, climate condition, lake level change and stable provenance are necessary conditions and controlling factors of the development of shallow water delta (Zhu et a.,2012; Zhu et al.,2013).

The semiarid-hot arid climate and the continuous uplift of the Bogeda Shan and Kelameili Shan may cause reductions in lake level and lake range (Fig. 15, Fig. 16, Fig. 17; Fig. 18). Moreover, the redox condition changed from weak anoxic/oxic conditions to intensive oxidizing conditions in response to changes in palaeosalinity, palaeoclimate and lake level (Fig. 18). Therefore, the lake gradually shrank from the centre to southwest of Fukang Sag during deposition of the Shishugou Group (Fig. 15, Fig. 16). The sedimentary system had never significantly changed due to the stable Kelameili Mountain provenance. The alluvial fans of Toutunhe Formation were only found in the front of Bogda Mountain because of the limited supply range of south provenance (Fig. 15, Fig. 16).

552 The west-southward gentle slope of the Fukang Sag, the relatively far Kelameili
553 Mountain provenance, the warm humid-hot arid climate condition and the low lake
554 level were beneficial to the development of a meandering river and shallow-water
555 meandering river delta (Fig. 15, Fig. 16, Fig. 18) (Postma, 1990; Lemons and Chan,
556 1999; Hoy and Ridgway, 2003; Cornel and Janok, 2006; Zhu et al., 2012; Zhu et al.,
557 2016). The gentle slope is the primary condition necessary for the formation of a
558 shallow-water meandering river delta. The palaeo-environment and provenance play a
559 critical role in the development and evolution of a shallow-water meandering river delta
560 (Fig. 16, Fig. 18).

561 The shallow-water meandering river delta can be divided into the humid delta and
562 the hot arid delta according to the climate conditions present (Zhu et al., 2012; Zhu et
563 al., 2016).The humid shallow-water delta is characterised by a “big front-small plain”
564 delta (BFBPD)(Fig. 16a) and the hot arid delta is characterized by a “big plain-small
565 front” delta (BPBFD) (Fig. 16b) (Zhu et al., 2012; Zhu et al., 2016). Therefore, the
566 depositional evolution from the “big front-small plain” shallow-water delta (BFBPD)
567 to the “big plain-small front” shallow-water delta (BPBFD) was controlled by the
568 change in climate and supply capacity of the sediment provenance (Fig. 16, Fig. 18).
569 The shallow-water meandering-river delta-plain environment rapidly changed into a
570 meandering river environment during the deposition of J_3q, which can be interpreted to
571 indicate that the hot arid climate conditions markedly reduced the lake level, lake range
572 and supply capacity of the sediment provenance (Fig. 16b-c, Fig. 18).

573 **6. Conclusions**

574 1. The redox conditions changed from weak anoxic/oxic into strong oxic conditions
575 during the deposition of the Middle-Late Jurassic Shishugou Group. The dominant

oxidizing conditions became more intense as strata age decreased.

2. The climate changed from warm-humid to hot-arid during the Middle-Late Jurassic in the Junggar Basin, which may have increased the salinity of the lake water and reduced the supply capacity of the sediment provenance.

3. The Kelameili Mountain provenance comprising northeastern and eastern Beisantai provenances, is the most important sediment source, but the south provenance, the Tianshan Mountains, (Bogeda Shan) supply sediments only for the very limited area of the southeastern Fukang Sag.

4. The gentle slope is the primary condition necessary for the formation of lake-shallow water delta-meandering river sedimentary systems, especially the shallow-water meandering river delta. The palaeo-environment and provenance play critical roles in the development and evolution of lake-shallow water delta-meandering river sedimentary systems.

Acknowledgement

We greatly thank the Western Research Institute, Shengli Oilfield Branch Company of Sinopec for providing all the related core samples, geological data and permission to publish these data. This work was funded by the Major Special Project for National Science and Technology [Grant numbers. 2016ZX05033-001-002], National Natural Science Foundation of China [Grant numbers. 41202043], and the China Scholarship Council (CSC). Finally, we especially thank the editors and reviewers for their work in improving the manuscript.

References

Algeo, T.J., & Twitchett, R.J. (2010). Anomalous Early Triassic sediment fluxes due to elevated weathering rates and their biological consequences. Geology, 38 (11), 1023–1026.

Algeo, T.J., Hinnov, L., Moser, J., Maynard, J.B., Elswick, E., Kuwahara, K., & Sano, H. (2010). Changes in productivity and redox conditions in the Panthalassic Ocean during the latest

602 Permian. Geology, 38 (2), 187–190.
603 Aubrecht, R., Sýkora, M., Uher, P., Li, X., Yang, Y., Putiš, M., & Plašienka, D. (2017). Provenance
604 of the Lunz Formation (Carnian) in the Western Carpathians, Slovakia: Heavy mineral study
605 and in situ LA–ICP–MS U–Pb detrital zircon dating. Palaeogeography, Palaeoclimatology,
606 Palaeoecology ,471, 233-253.
607 Bai, Y., Liu, Z., Sun, P., Liu, R., Hu, X., Zhao, H., & Xu, Y. (2015). Rare earth and major element
608 geochemistry of Eocene fine-grained sediments in oil shale- and coal-bearing layers of the
609 Meihe Basin, northeast China. Journal of African Earth Sciences， 97 (A)， 89–101.
610 Baioumy, H., & Lehmann, B. (2017). Anomalous enrichment of redox-sensitive trace elements in
611 the marine black shales from the Duwi Formation, Egypt: Evidence for the late Cretaceous
612 Tethys anoxia. Journal of African Earth Sciences, 133, 7-14.
613 Bassis, A., Hinderer,M., & Meinhold,G. (2016). New insights into the provenance of Saudi
614 Arabian Palaeozoic sandstones from heavy mineral analysis and single-grain geochemistry
615 Sedimentary Geology, 333, 100-114.
616 Berner, R.A. (1994). GEOCARB Ⅱ: a revised model of atmospheric CO2 over Phanerozoic time.
617 American Journal of Socience, 294, 56-91.
618 Bhatia, M.R. (1983). Plate tectonics and geochemical composition of sandstones. Journal of
619 Geology, 91, 611–627.
620 Bhatia, M.R., &Crook, K.A. (1986). Trace element characteristics of graywackes and tectonic
621 setting discrimination of sedimentary basins. Contributions to Mineralogy and Petrology, 92,
622 181–193.
623 Cao, J., Wu, M., Chan, Y., Hu, K., Bian, L. Z., Wang, L.G., & Zhang, Y. (2012). Trace and rare
624 earth elements geochemistry of Jurassic mudstones in the northern Qaidam basin, northwest
625 China. Chemie der Erde, 72, 245–252.
626 Cornel, O., & Janok, P.B. (2006). Terminal distributary channels and delta front architecture of
627 river dominated delta systems. Journal of Sedimentary Research, 76, 212-233.
628 Cross, T. A. (1994). High-resolution stratigraphic correlation from the perspective of base-level
629 cycles and sediment accommodation. In: Proceeding of Northwestern European Sequence

stratigraphy Congress, 105-123.

Cullers, R.L. (1995). The controls on the major- and trace-element evolution of shales,siltstones and sandstones of Ordovician to Tertiary age in the wet mountains region,Colorado, USA. Chemical Geology, 123, 107–131.

Deng, S., Lu, Y., Zhao, Y., Fan, R., Wang, Y., Yang, X., Li, X., & Sun, B. (2017). The Jurassic palaeoclimate regionalization and evolution of China. Earth Science Frontiers, 24,106-142 (in Chinese with English Abstract).

Dickinson, W.R., & Suczek, C.A. (1979). Plate tectonics and sandstone compositions. AAPG Bulletin, 63, 2164–2182.

Dinis, P.A., & Soares, A.F. (2007). Stable and ultrastable heavy minerals of alluvial to nearshore marine sediments from Central Portugal: Facies related trends. Sedimentary Geology, 201, 1-20.

Do Campo, M., Del Papa, C., Jiménez-Millán, J., & Nieto, F. (2007). Clay mineral assemblages and analcime formation in a Palaeogene fluvial-lacustrine sequence (Maíz Gordo Formation Palaeogen) from northwestern Argentina. Sedimentary Geology, 201, 56–74.

Do Nascimento Jr, D.R., Sawakuchi, A.O., Guedes, C.C.F., Giannini, P.C.F., Grohmann, C.H., & Ferreira, M.P. (2015). Provenance of sands from the confluence of the Amazon and Madeira rivers based on detrital heavy minerals and luminescence of quartz and feldspar. Sedimentary Geology, 316,1-12.

El-Sabbagh, A.M., El-Hedeny, M.M., & Mansour, A.S. (2017). Palaeoecology and palaeoenvironment of the Middle–Upper Jurassic sedimentary succession, central Saudi Arabia. Proceedings of the Geologists' Association, 128, 340-359.

Engelmanna, F. G., Chureb, J.D., & Fiorillo, R. A. (2004). The implications of a dry climate for the palaeoecology of the fauna of the Upper Jurassic Morrison Formation. Sedimentary Geology, 167, 297-308.

English, P.M. (2001). Formation of analcime and moganite at Lake Lewis, central Australia: significance of groundwater evolution in diagenesis. Sedimentary Geology, 143,219–244.

Fisk, H. N. (1954). Sedimentary framework of the modern Mississippi delta. Journal of Sedimentary

Petrology, 24(2):76-99.

Floyd, P.A., Keele, B.E., Leveridge, B.E., Franke,W., Shail, R., & Dörr, W. (1990). Provenance and depositional environment of Rhenohercynian synorogenic greywackes from the Giessen Nappe, Germany. Geologische Rundschau, 79 (3), 611–626.

Galarragaa, F., Reateguia, K., Martïneza, A., Martíneza,M., Llamas,J,F., & Márquez,G.(2008). V/Ni ratio as a parameter in palaeoenvironmental characterisation of nonmature medium-crude oils from several Latin American basins. Journal of Petroleum Science and Engineering,61,9-14.

Galloway, J.M., Sweet, A.R., Swindles, G. T., & Dewing, K. (2013). Middle Jurassic to Lower Cretaceous palaeoclimate of Sverdrup Basin, Canadian Arctic Archipelago inferred from the palynostratigraphy. Marine and Petroleum Geology, 44, 240-255.

Garzanti, E., Andò, S., & Vezzoli, G. (2008). Settling-equivalence of detrital minerals and grain size dependence of sediment composition. Earth and Planetary Science Letters, 273, 138–151.

Gong, Q. (2015). Sedimentary characteristics and tectonic background of the Jurassic in the south and east margin of the Junggar basin. (Master thesis) China University of geosciences, Beijing, China, 59-62 (in Chinese with English Abstract).

Graver, J.I., &and Scott, T.J. (1995). Trace elements in shale as indicators of crustal province and terrain accretion in the southern Canadian Cordillera. Geological Society of America Bulletin, 107, 440–453.

Greene, T. J., Carroll, A. R., Hendrix, M. S., Graham, S.A., & Warters, M.A. (2001). Sedimentary record of Mesozoic deformation and inception of the Turpan-Hami basin, northwest China. In: Hendrix, M.S., Davis, G. A. (Eds.), Palaeozoic and Mesozoic Tectonic Evolution of Central Asia: From continental assembly to intracontinental deformation. Geological Society of America Memoir, 194,317-340.

Grome, L.P., Haskin,L.A., Korotev , R. L., &Dymek, R. F.,(1984). The “North American shale composite”: Its compilation, major and trace element characteristics. Geochimica et Cosmochimica Acta,48(12),2469-2482. Harrell, JR.T. L & Pe´rez-Huerta, A. (2015). Rare Earth elements (REE) analysis of vertebrate fossils from the Upper Cretaceous Carbonate

686 marine formations of western and central Alabama, USA: Taphonomic and
687 Paleoenvironmental implications. PALAIOS, 30,514-528.
688 Hartley, A., Flint, S., & Turner, P. (1991). Analcime: a characteristic authigenic phase of Andean
689 alluvium, northern Chile. Geological Journal, 26, 189–202.
690 Hoy, R.G., & Ridgway, K.D. (2003). Sedimentology and sequence stratigraphy of fan delta and
691 river delta deposystems, Pennsylva-nian Minturn Formation, Colorado. AAPG Bulletin, 87 (7),
692 1169-1191.
693 Huber, B.T., MacLeod, K. G., & Wing, S.T. (2000). Warm Climates in Earth History. Cambridge
694 University Press, Cambridge.
695 Ji, J., Wen, H., Xiang, B., Qi, L., Yu, J., & Li, L. (2014). Provenance analysis of Middle Jurassic
696 Toutunhe Formationin eastern Fukang slope, Junggar Basin. Lithological Reservoir, 26(2), 54-
697 59(in Chinese with English abstract).
698 Jin, B., Lin, Z., Yang, Q., & Ji, F. (2002). Application of sedimentary mineralogy to the
699 environmental analysis in marginal seas. Marine Geology & Quaternary Geology, 22(3), 113-
700 118.
701 Jone, J. S., Arzani, N., & Allen, B.M. (2014). Tectonic and climatic controls on fan systems: The
702 Kohrudmountain belt,Central Iran. Sedimentary Geology, 302, 29-43.
703 Jones, B., & Manning, D. A. C. (1994). Comparison of geochemical indices used for the
704 interpretation of palaeoredox conditions in ancient mudstones. Chemical Geology ,111,111-
705 129.
706 Kim, B., Cheong, D., &Lee, E. (2015). Palaeoenvironmental changes in northern Mongolia during
707 the last deglaciation revealed by trace element records in ostracods from Lake Hovsgol.
708 Quaternary International, 384,169-179.
709 Kuzyk, Z.Z.A., Gobeil,C., Goni, M. A., & Macdonald, R.W. (2016). Early diagenesis and trace
710 element accumulation in North American Arctic margin sediments. Geochimica et
711 Cosmochimica Acta, 203, 175-200.
712 Lemons, D. R., &Chan, M. A . (1999) .Facies architecture and sequence stratigraphy of fine-
713 grained lacustrine deltas along the eastern margin of late Pleistocene Lake Bonneville，northern

714 Utah and southern Idaho. AAPG Bulletin，83(4) : 635-665.
715 Lee, Y.I. (2009). Geochemistry of shales of the Upper Cretaceous Hayang Group, SE Korea:
716 implications for provenance and source weathering at an active continental margin.
717 Sedimentary Geology, 215, 1–12.
718 Lemons, D.R., & Chan, M.A. (1999). Facies architecture and sequence stratigraphy of fine
719 grained lacustrine deltas along the eastern margin of late Pleistocene Lake Bonneville, northern
720 Utah and southern Idaho. AAPG Bulletin, 83 (4), 635-665.
721 Lerman, A. (1978). Chemistry, Geology and Physics of Lake. Springer- Verlag, New York,
722 Heidelberg Berilin.
723 Li, P., Zou, H., & Hao, F. (2006). Formation Mechanism and effect on petroleum accumulation of
724 the weathering crust top of Jurassic in the Hinterland of Junggar Basin. Acta Sedimentolohica
725 Sinica, 24(6), 889-896 (in Chinese with English abstract).
726 Lin, Z., Chen, D., & Liu, Q. (2008). Geochemical indices for redox conditions of marine
727 sediments. Bull. Mineral. Petrology and Geochemistry, 27(1), 72-80.
728 Liu, D., Kong, X., Zhang, C., Wang, J., Yang, D., Liu, X., Wang, X., & Song, Y. (2018).
729 Provenance and geochemistry of Lower to Middle Permian strata in the southern Junggar and
730 Turpan basins: A terrestrial record from mid-latitude NE Pangea. Palaeogeography,
731 Palaeoclimatology, Palaeoecology, 495, 259-277.
732 Liu, Y. (2012). Lower Jurassic heavy minerals from southern Mt. Hala'alate，Junggar Basin:
733 Characteristics and geological implications. Sedimentary Geology and Tethyan Geology, 32(4):
734 34-37.
735 Luo, L., Gao, X., Meng, W., Tan, X., Shao, H., & Xiao, C. (2018). The origin and alteration of
736 calcite cement in tight sandstones of Jurassic Shishugou Group in the Fukang Sag, Junggar
737 Basin, NW China: Implications for fluid–rock interactions and porosity evolution. Australian
738 Journal of Earth Sciences, 65(3),427-445.
739 Lv, D., &Chen, J. (2014). Depositional environments and sequence stratigraphy of the Late
740 Carboniferous - Early Permian coal-bearing successions (Shandong Province, China):
741 Sequence development in an epicontinental basin. Journal of African Earth Sciences, 79, 16-

742 30.
743 Lv,D., Zong, R., Li, Z., Wang, D., Liu, H., Wu, X., Wang, X., Yu, D., Feng, T., Zhao, L., Yang, Q.,
744 & Yong, P. (2016).Oil shale paleo-productivity disturbed by sea water in a coal and oil shale
745 bearing succession: A case study from the Paleogene Huangxian basin of Eastern China.
746 Journal of Petroleum Science and Engineering, 139, 62-70.
747 Lv, D., Wang, D., Li, Z., Liu, H., & Li, Y. (2017). Depositional environment, sequence stratigraphy
748 and sedimentary mineralization mechanism in the coal bed- and oil shale-bearing succession:
749 A case from the Paleogene Huangxian Basin of China. Journal of Petroleum Science and
750 Engineering 148: 32-51.
751 Martínez-Yáñez, M., Núñez-Useche,F., & Martínez,R.L.(2017). Palaeoenvironmental conditions
752 across the Jurassic–Cretaceous boundary in central-eastern Mexico. Journal of South American
753 Earth Sciences, 77, 261-275.
754 McCulloch, M.T., & Wasserburg, G.J. (1978). Sm–Nd and Rb–Sr chronology of continental crust
755 formation. Science, 200, 1003–1011.
756 McLennan, S.M., & Taylor, S.R. (1991). Sedimentary rocks and crustal evolution: tectonic setting
757 and secular trends. Journal of Geology, 99,1–21.
758 McLennan, S.M., Taylor, S.R., & Eriksson, K.A. (1983). Geochemistry of Archean shales from
759 the Pilbara Supergroup, Western Australia. Geochimica et Cosmochimica Acta, 47,1211–1222.
760 McLennan, S.M., Hemming, S., McDaniel, D.K., & Hanson, G.N. (1993). Geochemical
761 approaches to sedimentation, provenance, and tectonics. Geological Society of America
762 Special Papers, 284, 21–40.
763 Meng, Q.T., Liu, Z.J., Bruch, A.A., Liu,R., & Hu, F. (2012). Palaeoclimatic evolution during the
764 Eocene and its influence on oil shale mineralisation, Fushun Basin, China. Journal of African
765 Earth Sciences, 45, 95–105.
766 Moore, G.T., Hayashida, D.N., Ross, C.A., & Jacobson, S. R. (1992).Palaeoclimate of the
767 Kimmeridgian/Tithonian (Late Jurassic) world: I. Results using a general circulation model.
768 Palaeogeography, Palaeoclimatology, Palaeoecology, 93,113-150.
769 Moradi, A.V., Sarı, A., & Akkaya, P. (2016). Geochemistry of the Miocene oil shale (Hançili

770 Formation) in the Çankırı-Çorum Basin, Central Turkey: Implications for Palaeoclimate
771 conditions, source–area weathering, provenance and tectonic setting. Sedimentary Geology,
772 341, 289–303.
773 Moreno, C.J., Caballero, V., & Parra, M. (2012). Integrated provenance analysis of a convergent
774 retroarc foreland system: U–Pb ages, heavy minerals, Nd isotopes, and sandstone compositions
775 of the Middle Magdalena Valley basin, northern Andes, Colombia. Earth-Science Reviews,
776 110,111–126.
777 Morton, A.C., & Hallsworth, C.R. (1999). Processes controlling the composition of heavy mineral
778 assemblages in sandstone. Sedimentary Geology, 124, 3–29.
779 Morton, A.C., Meinhold,G., Howard,J.P., Phillips,R.J., Strogen,D., Abutarruma,Y., Elgadry,M.,
780 Thusu,B., & Whitham,A.G. (2011). A heavy mineral study of sandstones from the eastern
781 Murzuq Basin, Libya: Constraints on provenance and stratigraphic correlation. Journal of
782 African Earth Sciences, 61, 308-330.
783 Murray, R.W., Buchholtz ten Brink, M.R., Gerlach, D.C., Russ,D.P., & Jones, D.L. (1992).
784 Interoceanic variation in the rare earth, major, and trace element depositional chemistry of chert:
785 Perspectives gained from the DSDP and ODP record. Geochimica et Cosmochimica Acta, 56,
786 1897–1913.
787 Murthy, R., Kidder, D., Mapes, R., & Hannigan, R. (2004). Rare-earth element chemistry of
788 Mississippian–age phosphate nodules in the Fayetteville Shale of Oklahoma and Arkansas.
789 Environmental Geosciences, 11(2), 99-111.
790 Myers, T.S., Tabor, N.J., & Jacobs, L.L. (2011). Late Jurassic palaeoclimate of Central Africa.
791 Palaeogeography, Palaeoclimatology, Palaeoecology, 311(1-2), 111-125.
792 Nesbitt, H.W., &Young, G.M. (1982). Early Proterozoic climates and plate motions inferred from
793 major element chemistry of lutites. Nature, 299, 715–717.
794 Nie, J.S., Horton, B.K., Saylor, J.E., Mora, A., Mange, M., Garzione, C.N., Basu, A.,Moreno, C.J.,
795 Caballero, V., & Parra, M. (2012). Integrated provenance analysis of a convergent retroarc
796 foreland system: U–Pb ages, heavy minerals, Nd isotopes, and sandstone compositions of the
797 Middle Magdalena Valley basin, northern Andes, Colombia. Earth-Science Reviews, 110, 111–

126.

Owen, A.W., Armstrong, H.A., & Floyd, J. D. (1999).Rare earth elements in chert clasts as provenance indicators in the Ordovician and Silurian of the Southern Uplands of Scotland. Sedimentary Geology, 124,185-195.

Pi, D.H., Jiang, S.Y., Luo, L., Yang, J.H., & Ling, H.F. (2014). Depositional environments for stratiformwitherite deposits in the Lower Cambrian black shale sequence of the Yangtze Platform, southern Qinling region, SWChina: evidence from redox-sensitive trace element geochemistry. Palaeogeography, Palaeoclimatology, Palaeoecology, 398, 125-131.

Postma, G. (1990). An analysis of the variation in delta architecture. Terra Nova 2(2), 124-130.

Potter-McIntyre, S.L., Boraas, M., DePriest,K., & Aslan,A. (2016).Middle Jurassic landscape evolution of southwest Laurentia using detrital zircon geochronology. Lithosphere, 8,185-193.

Rimstidt, J.D., Chermak, J.A., & Schreiber, M.E. (2017). Processes that control mineral and element abundances in shales. Earth-Science Reviews, 171, 383-399.

Roser, B.P., & Korsch, R.J. (1986). Determination of tectonic setting of sandstone–mudstone suites using SiO2 content and K2O/Na2O ratio. Journal of Geology, 94, 635–650.

Sellwood, B.W., & Valdes, P.J. (2008). Jurassic climates. Proceedings of the Geologists Association, 119, 5-17.

Sevastjanova, I., Hall, R., & Alderton, D. (2012). A detrital heavy mineral viewpoint on sediment provenance and tropical weathering in SE Asia. Sedimentary Geology, 280,179-194.

Shang, L., Dai, J., Liu,X., &Bian,B.(2011). Sedimentary source analysis of Jurassic Toutunhe Formation in Beisantai area in Junggar Basin. Global Geology,30(4),579-584(in Chinese with English abstract).

Sochava, A.V., Podkovyrov, V.N., & Felitsyn, S.B. (1994). Late Precambrian evolution of terrigenous rock composition. Stratigraphy and Geological Correlation, 2, 3–21.

Souto, P.R.F., & Fernandes, M.A. (2017). Palaeobiogeographical significance of the Late Jurassic continental fauna from western Gondwana. Palaeoworld, 26, 230-240.

Su, Z., Chen, L., Xu, T., Zhang, M., Zhang, R., &Xiu, J. (2014). Provenance system research of

Jurassic Toutunhe Formation in 2,4 blocks of the middle of Junggar Basin. Petroleum Geology and Engineering, 28（2），9-11 (in Chinese with English abstract).

Svendsen,J.B., & Hartley, N.R. (2002). Synthetic heavy minerals stratigraphy: applications and limitations. Marine and Petroleum Geology, 19, 389–405.

Sverjensky, D. A. (1984). Europium redox equilibria in aqueous solution. Earth and Planetary Science Letters, 67, 70–78.

Tan, M., Zhu, X., Geng, M., Zhu, S., & Liu, W. (2017). The occurrence and transformation of lacustrine sediment gravity flow related to depositional variation and paleoclimate in the Lower Cretaceous Prosopis Formation of the Bongor Basin, Chad. Journal of African Earth Sciences, 134, 134-148.

Tanaka, K., Akagawa, F., Yamamoto, K., Tani, Y., Kawabe, I., & Kawai, T. (2007). Rare earth element geochemistry of Lake Baikal sediment: its implication for geochemical response to climate change during the Last Glacial/Interglacial transition. Quaternary Science Reviews, 26 (9), 1362–1368.

Tribovillard, N., Algeo, T. J., Lyons, T., & Riboulleau, A. (2006). Trace metals as palaeoredox and palaeoproductivity proxies –An update. Chemical Geology, 232,12 -32.

Vernet, J.P. (1961). Concerning the association montmorillonite–analcime in the series of Stanleyville, Congo. Journal of Sedimentary Research, 31 (2), 293–295.

Wang, X., Hou, J., Song, S., Wang, D., Gong, L., Ma, K., Liu, Y., Li, Y., & Yan, L. (2018). Combining pressure-controlled porosimetry and rate-controlled porosimetry to investigate the fractal characteristics of full-range pores in tight oil reservoirs. Journal of Petroleum Science and Engineering, 171, 353-361.

Wang, Y., Wang, Y., Qi, X., Guan, S., Zhao, X., & Li, R. (2001). Classification of stratigraphic sequences of Jurassic in Junggar Basin. Xinjiang Petroleum Geology, 22(5), 382-385.

Wierzbowski, H., Rogov, M.A., Matyja, B.A., Kiselev, D., & Ippolitov, A. (2013). Middle–Upper Jurassic (Upper Callovian–Lower Kimmeridgian) stable isotope and elemental records of the Russian Platform: Indices of oceanographic and climatic changes. Global and Planetary Change, 107, 196-212.

853 Wignall, P.B., & Twitchett, R.J. (1996). Oceanic anoxia and the end Permian mass extinction.
854 Science, 272, 1155-1158.
855 Wilde, P., Quibabyhunt, M. S., &Erdtmann, B. D.,1996. The whole-rock Cerium anomaly : A
856 potential indicator eustatic sea-level changes in shales of anoxic facies. Sedimentary Geology,
857 101，43-53.
858 Worash, G. (2002). Geochemistry provenance and tectonic setting of the Adigrat sandstone northern
859 Ethiopia. Journal of African Earth Sciences, 35, 185–198.
860 Wu, Q. (1986). Development stage tectonic units and origin of local structure of Junggar Basin.
861 Xinjiang Petroleum Geology, 7(1), 29-37 (in Chinese with English abstract).
862 Yan, Y., Xia, B., Lin, G., Cui, X., Hu, X., Yan, P., & Zhang, F. (2007). Geochemistry of the
863 sedimentary rocks from the Nanxiong Basin,South China and implications for provenance,
864 palaeoenvironment and palaeoclimate at the K/T boundary. Sedimentary Geology, 197, 127-
865 140.
866 Yu, J., Liu, N., Wen, H., Zhu, R., & Zhang, Z. (2016). Analysis of high-resolution sequence
867 stratigraphy and prediction of favorable sandbodies in the Upper Jurassic Qigu Formation in
868 Fudong slope area，Junggar Basin. Journal of Palaeogeography, 18(2), 265-274 (in Chinese
869 with English abstract).
870 Yu, J., Zheng, R., Qi, L., Zhang, Z., Wen, H., & Li, Y.2014. Precise Analysis on High-resolution
871 Sequence Stratigraphy and Micro-facies of Toutunhe Formation of Middle Jurassic in the East
872 Slope Zone，Fukang Sag，Junggar Basin. Geological Review, 60(6), 1337-1347 (in Chinese
873 with English abstract).
874 Zhang, B.M., Chen, J.P., Bian, L.Z., & Zhang, S.C. (2006). Rediscussion on the sea-looding
875 events during Triassic to Jurassic of Kuqa Depression in Tarim Basin. Acta Geol. Si Acta
876 Geologica Sinica, 80, 236–244 (in Chinese with English abstract).
877 Zhang, Q., Zhang, M., Zhu, X., Zhong, D., &Wang, G. (1999). Analysis of Jurassic Sources in
878 Fukang of Junggar Basin.Xinjiang Petroleum Geology, 20 (6),501-504 (in Chinese with
879 English abstract).
880 Zhang, M., Zhang, Q., Zhu, X., Li, X., & Wang, J. (2000). Sequence stratigraphy of Jurassic on

881 the east Fukang slope,Junggar Basin. Journal of Palaeogeography, 2(3), 27-36 (in Chinese with
882 English abstract).
883 Zhang, X., Lin, C., Zahid, M.A., Jia, X., & Zhang, T. (2017).Palaeosalinity and water body type
884 of Eocene Pinghu Formation, Xihu Depression, East China Sea Basin. Journal of Petroleum
885 Science and Engineering, 158, 469-478.
886 Zhao, Z.Y., Zhao, J.H., Wang, H.J., Liao, J.D., & Liu, C.M. (2007). Distribution characteristics
887 and applications of trace elements in Junggar Basin. Natural Gas Exploration and Development,
888 30,30–33 (in Chinese with English abstract).
889 Zhu, X., Li, S., Wu, D., Zhu, S., Dong, Y., Zhao, D., Wang, X., & Zhang, Q. (2017). Sedimentary
890 characteristics of shallow-water braided delta of the Jurassic, Junggar basin, Western China
891 Journal of Petroleum Science and Engineering, 149, 591-602.
892 Zhu, X., Pan, R., Zhao, D., Liu, F., Wu, D., Li, Y., &Wang, R. (2013). Formation and development
893 of shallow-water deltas in lacustrine basin and typical case analyses. Journal of China
894 University of Petroleum,37(5),7-14(in Chinese with English abstract).
895 Zhu, X., Liu, Y., Fang, Q., Li, Y., Liu, Y., Wang, R., Song, J., Liu, S., Cao, H., & Liu, X. (2012).
896 Formation and sedimentary model of shallow delta in large scale lake, example from
897 Cretaceous Quantou Formation in Sanzhao Sag, Songliao Basin. Earth Science Frontiers, 19
898 (1), 089-099 (in Chinese with English abstract).
899 Zhu, X., Zhong, D., Yuan, X., Zhang, H., Zhu, S., Sun, H., Gao, Z., & Xian, B. (2016).
900 Development of sedimentary geology of petroliferous basins in China. Petroleum Exploration
901 & Development, 43(5), 820-829 (in Chinese with English abstract).
902 Zou, Z., Yu, C., & Chen, H. (2014). Sedimentary Characteristics of Toutunhe Formation 2nd
903 Member on East Fukang Slope of Junggar Basin. Xinjiang Geology, 32(2), 214-218 (in
904 Chinese with English abstract).
905

Figure captions

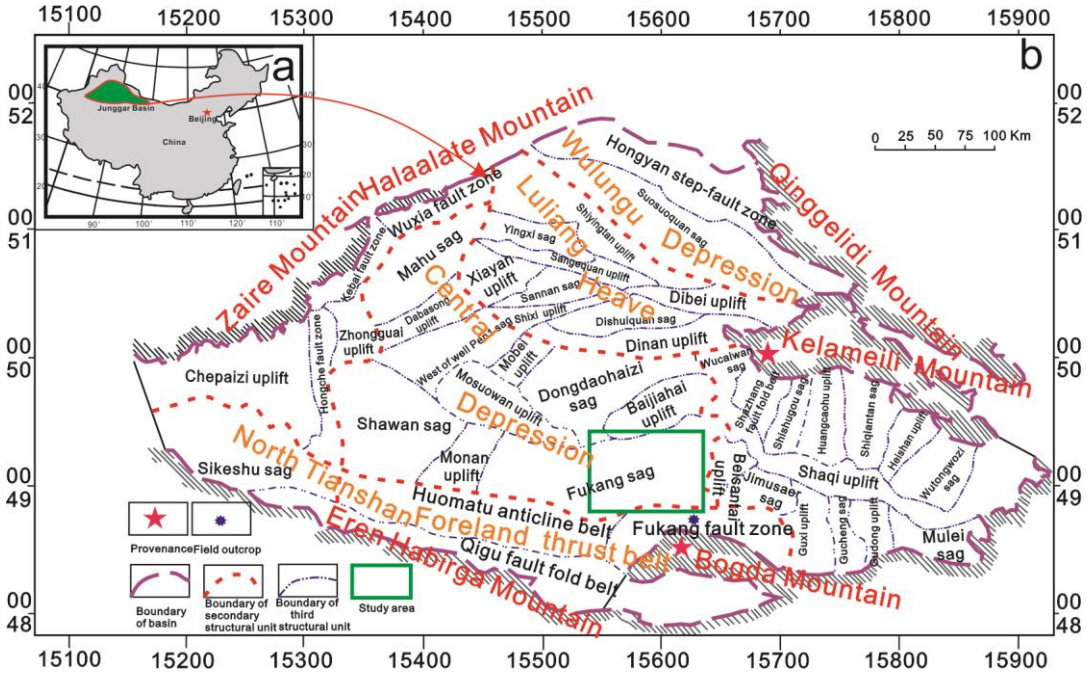

Fig. 1. Maps showing the (a) Location of the Junggar Basin in China and (b) Location of the Fukang Sag

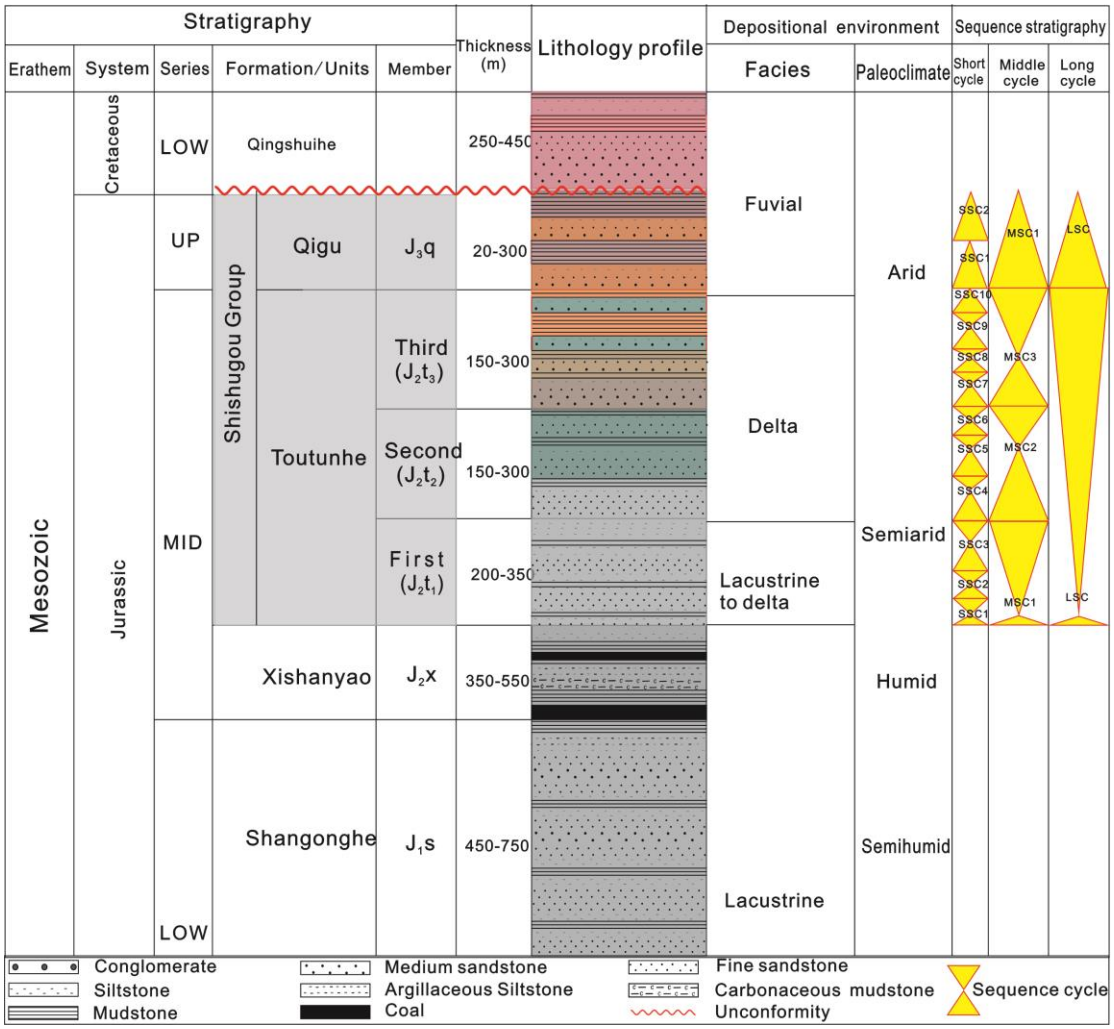

Fig. 2. Stratigraphic column of the Fukang Sag of Junggar Basin showing the Shishugou Group (the Toutunhe and Qigu Formations).

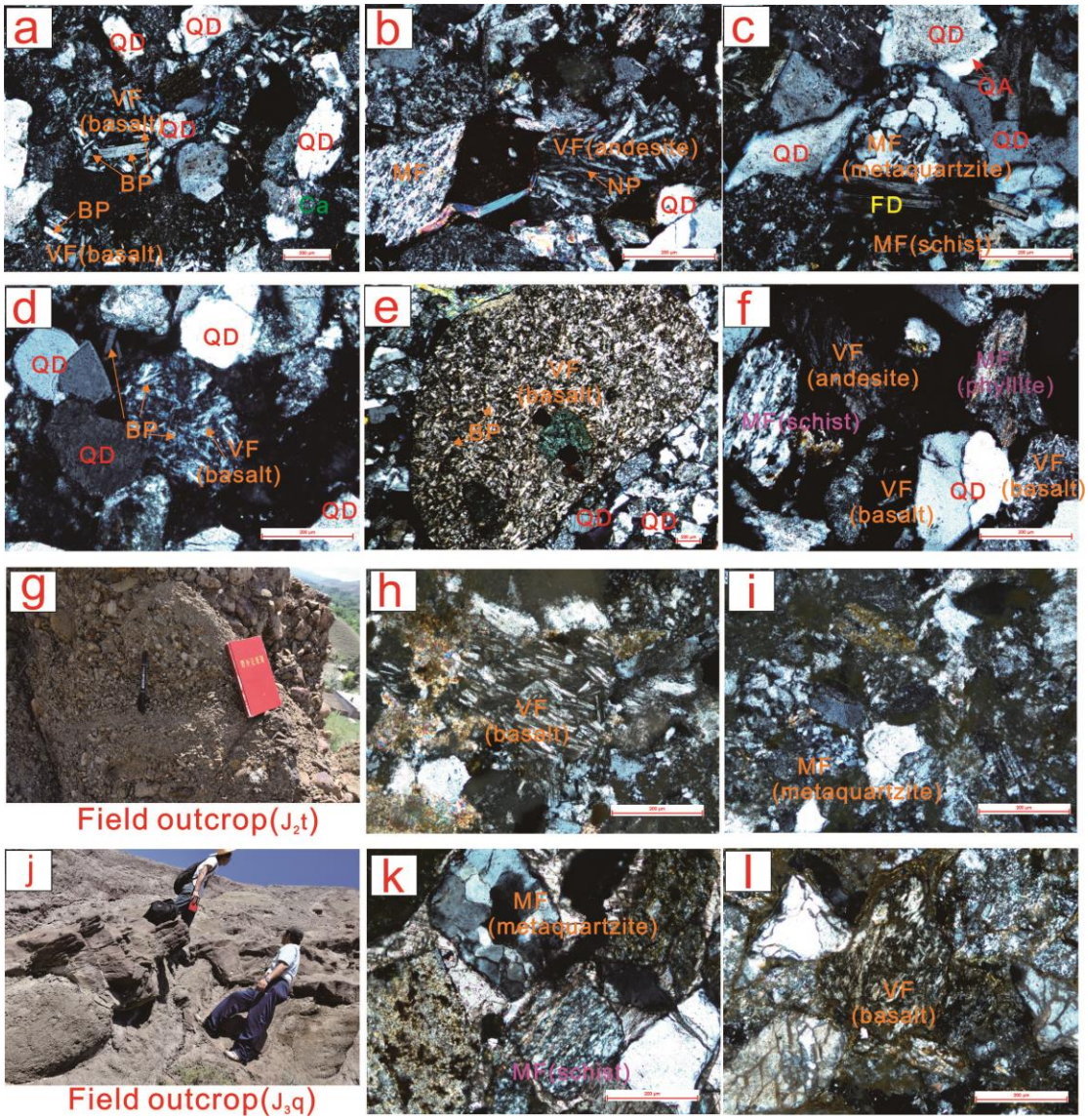

Fig. 3. Petrological and mineralogical characteristics of the Shishugou Group sandstone, detrital quartz -QD (based on Luo et al.,2018)：(A) Micrograph of thin section showing the volcanic rock fragment (VF) comprising basalt fragments characterized by porphyritic texture with bundles or radial pattern of lath-shaped basic plagioclase phenocryst (BP), well D7, 4517.6m, J_2t. (B) Micrograph of thin section showing andesite fragments (VF) characterized by porphyritic texture with directionally arranged neutral plagioclase phenocryst (NP),well D7,4133.4m, J_2t. (C) Micrograph of thin section showing the metamorphic rock fragment (MF) consisting of metaquartzite and schist , quartz

928 overgrowth (QA) and feldspar (FD),well D8,4545.4m, J_2t.(D) Micrograph of thin
929 section showing the basalt fragments (VF) characterized by porphyritic texture
930 with radial distribution of lath-shaped basic plagioclase phenocryst (BP), well
931 D6, 4257.65m, J_3q. (E) Micrograph of thin section showing the basalt fragments
932 (VF) characterized by porphyritic texture with radial distribution of lath-shaped
933 basic plagioclase phenocryst (BP),well D701,3902.95m, J_3q. (F) Micrograph of
934 thin section showing the volcanic rock fragment (VF) including basalt and
935 andesite fragments and the metamorphic rock fragment (MF) comprising schist
936 and phyllite, well D6,4257.65m, J_3q. (G) Photograph of conglomerate of the J_2t
937 in the Sangonghe field outcrop (Fig. 1) showing existence of south
938 provenance.(H) Micrograph of conglomerate collected from the outcrop of G
939 showing that rock fragment comprising volcanic (basalt) rock fragment (VF). (I)
940 Micrograph of conglomerate collected from the outcrop of G showing that rock
941 fragment comprising metamorphic (Metaquartzite) rock fragment (MF). (J)
942 Photograph of the J_3q in the Sangonghe field outcrop (Fig. 1) showing the
943 channel deposit with sandstone lens. (K) Micrograph of sandstone collected from
944 the outcrop of J showing that rock fragment comprising metamorphic
945 (Metaquartzite) rock fragment (MF). (L) Micrograph of sandstone collected from
946 the outcrop of J showing that rock fragment comprising volcanic (basalt) rock
947 fragment (VF).

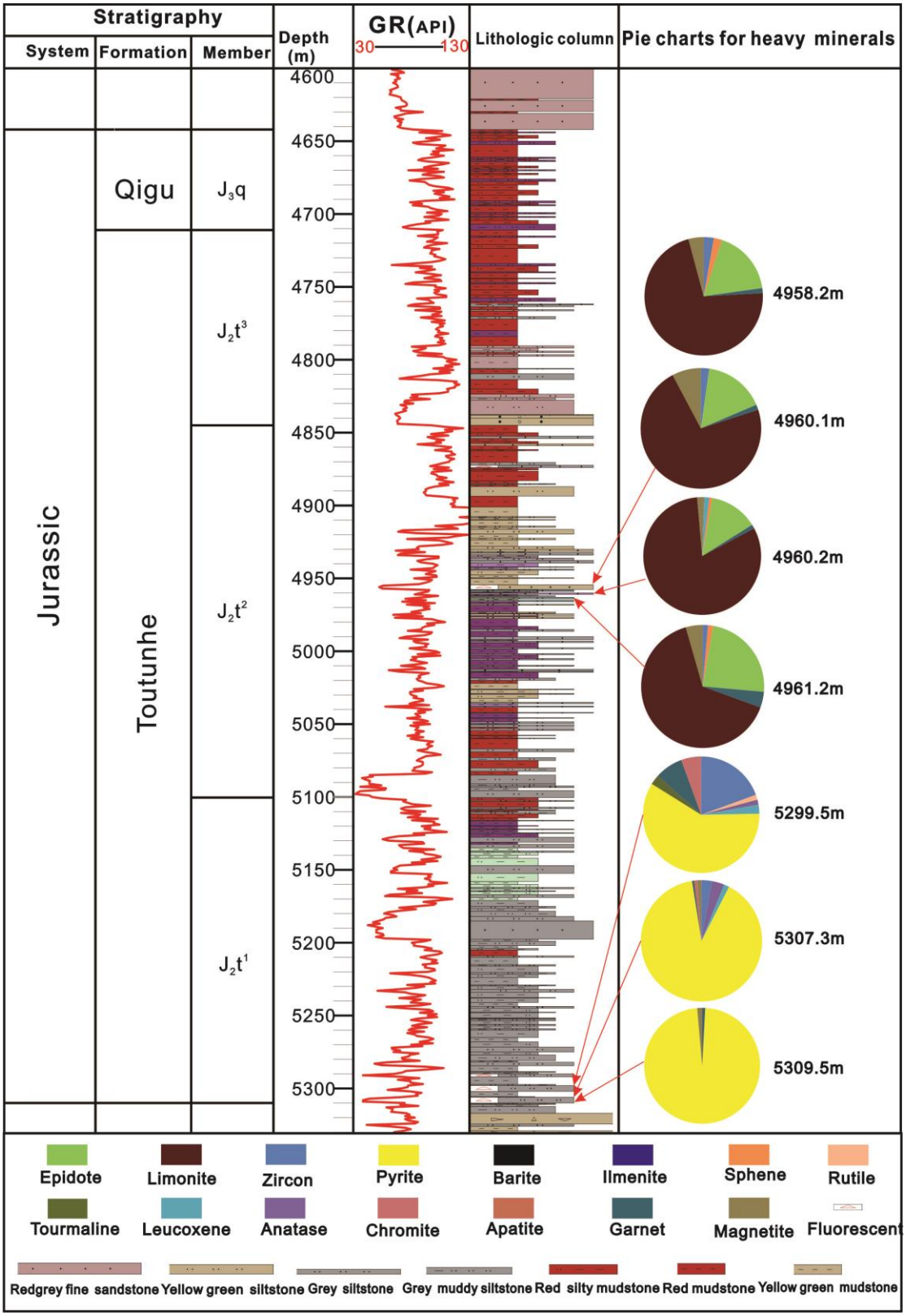

Fig. 4 Percentage distribution of heavy minerals in the Shishugou Group sandstones of well D1

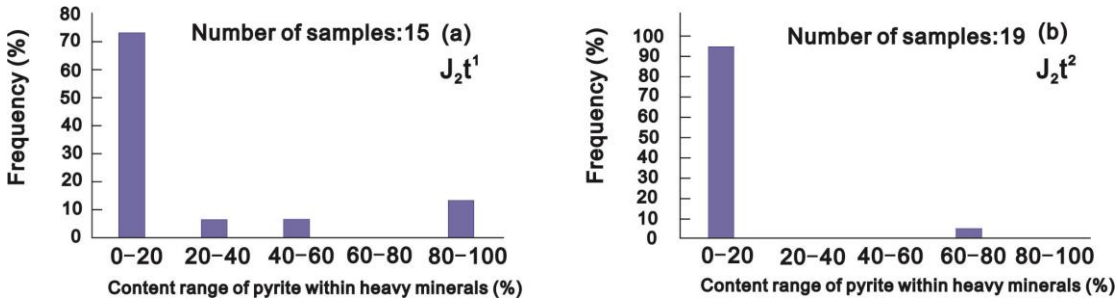

952
953 Fig. 5 The relative content of pyrite in the heavy mineral component of different
954 strata. a: content range of pyrite in heavy minerals in J_2t^1. b: content range of
955 pyrite in heavy minerals in J_2t^2.
956

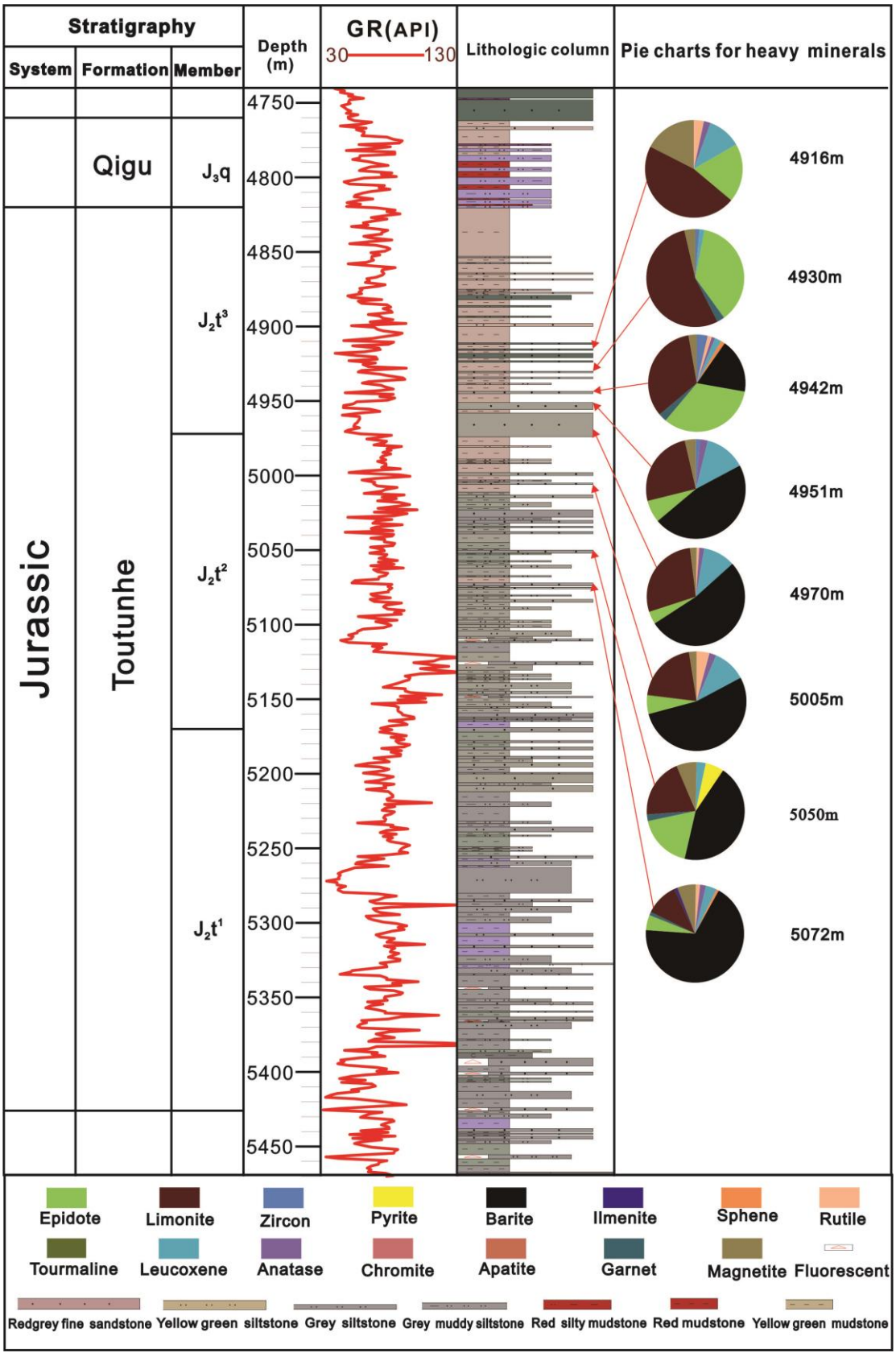

957

958 Fig. 6 Percentage distribution of heavy minerals in the Shishugou Group sandstones

959 of well D101

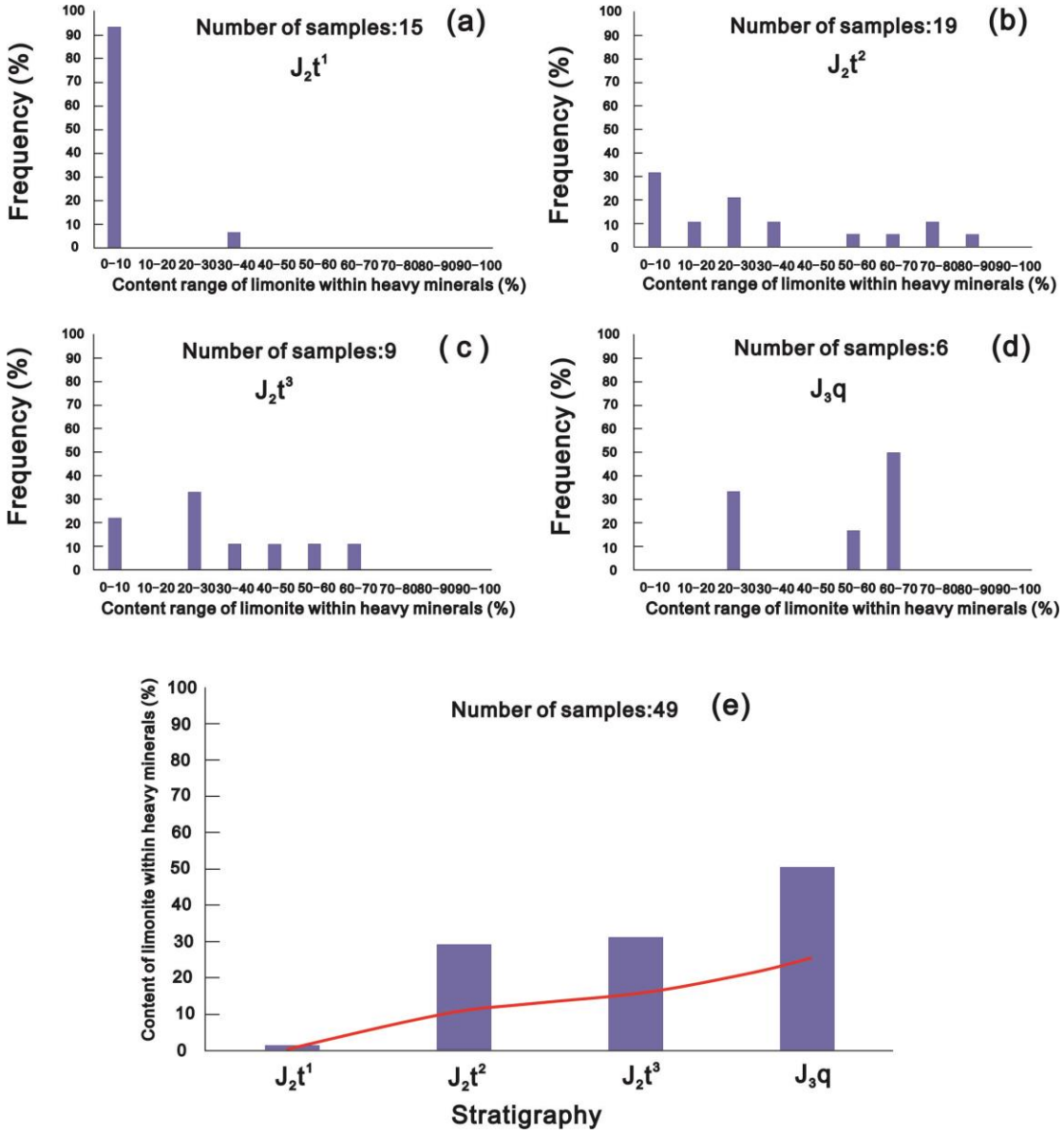

Fig. 7 Limonite content of heavy minerals in different strata. A: content range of limonite within heavy minerals in the J_2t^1 stratum. B: content range of limonite within heavy minerals in the J_2t^2 stratum. C: content range of limonite within heavy minerals in the J_2t^3 stratum. D: content range of limonite within heavy minerals in the J_3q stratum. E: content change of limonite within heavy minerals in different strata.

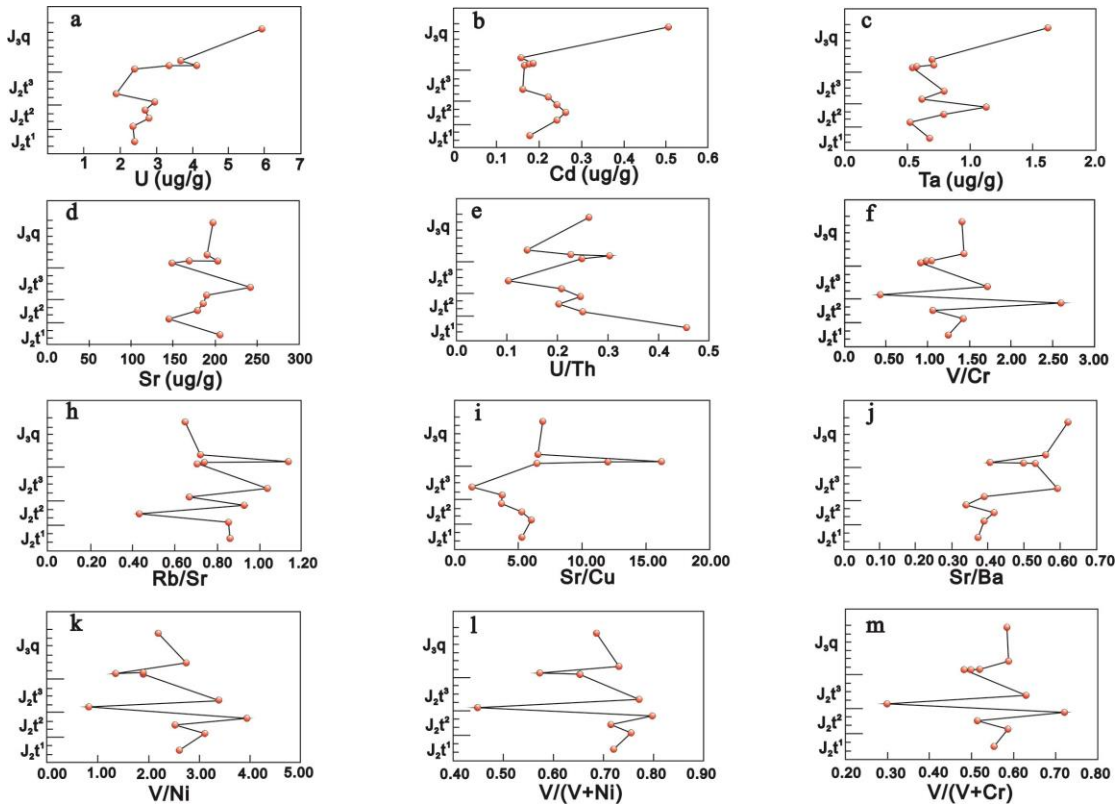

968

969 Fig. 8 Vertical change of trace elements and ratios in the Shishugou Group mudstone

970

971

972

973

974

975

976

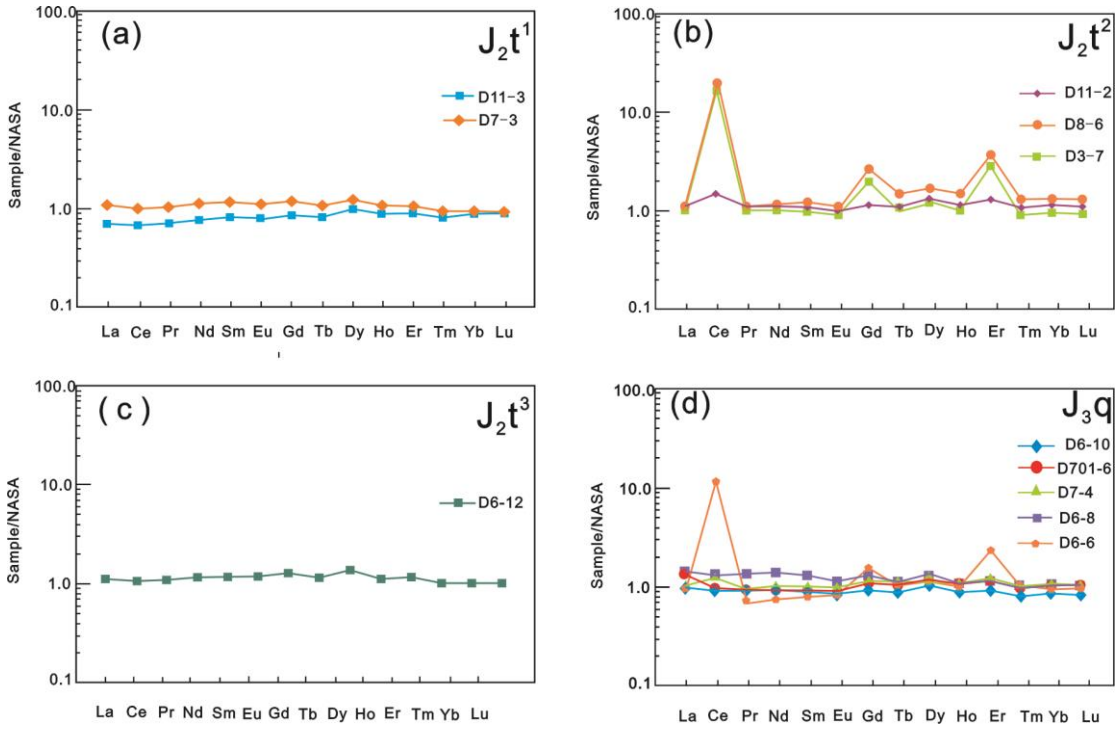

977

978 Fig. 9 NASA -normalised rare earth element (REE) patterns for the mudstone samples

979 from J_2t^1 (a), J_2t^2 (b), J_2t^3 (c) and J_3q (d).

980

981

982

983

984

985

986

987

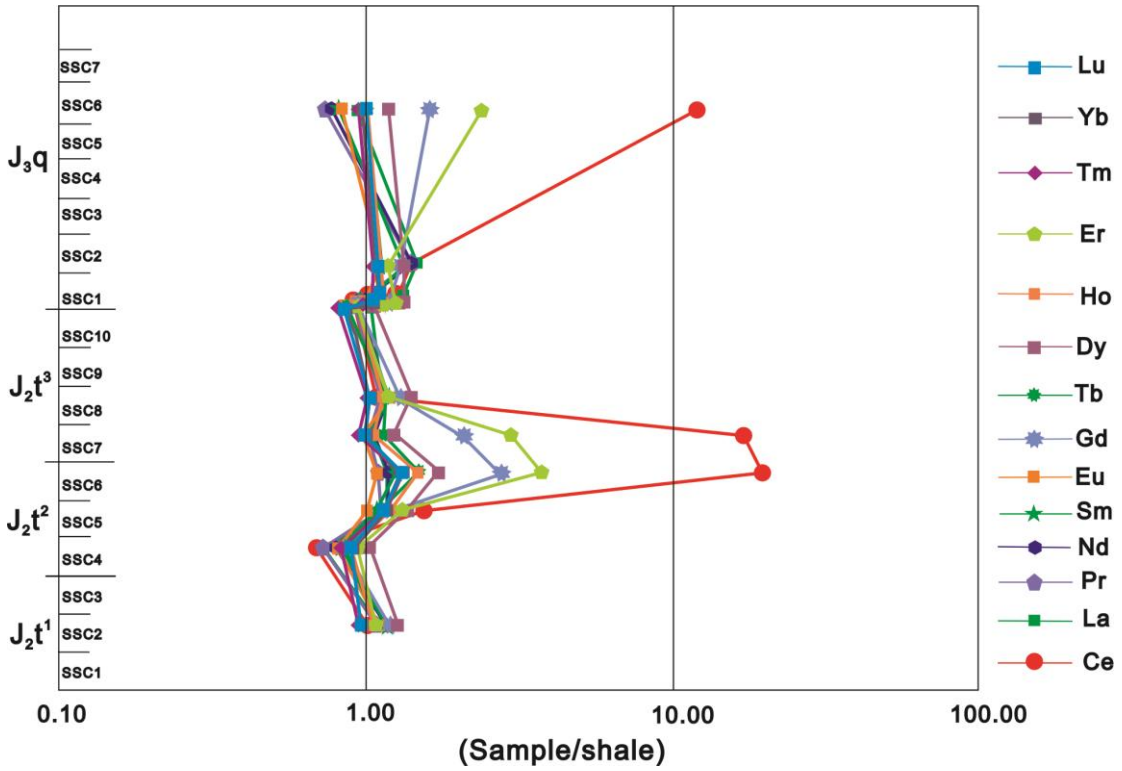

988

989 Fig. 10 Vertical change of shale-normalised (NASA) rare earth element (REE) in the

990 Shishugou Group mudstone

991

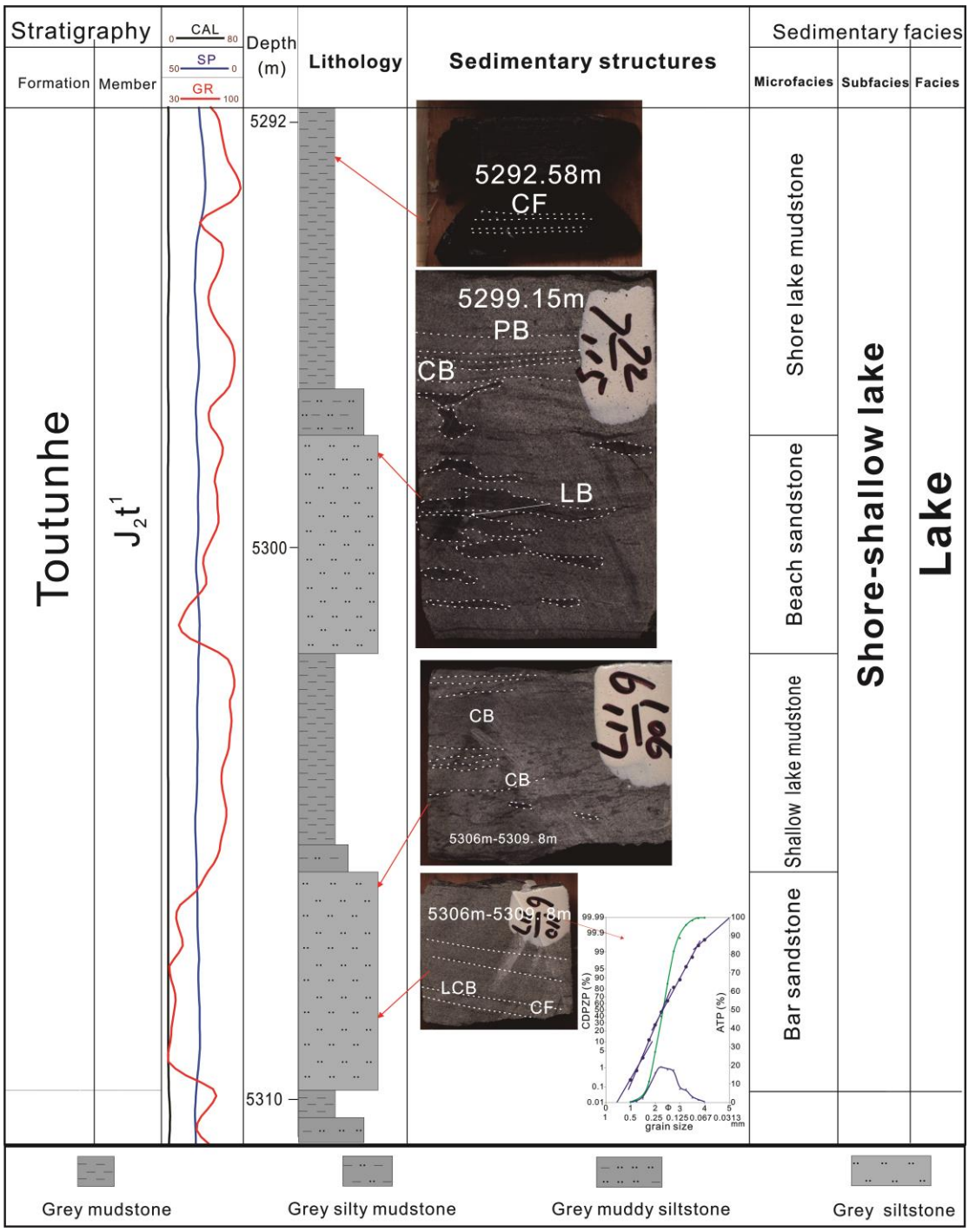

Fig. 11 Lithofacies, logging characteristics, sedimentary structures and sedimentary facies analysis of facies association A.CF= Carbon fragment; PB=Parallel bedding; CB= Current bedding; Lenticular bedding; LCB=Low-angle cross bedding; CDPZP=Cumulative distribution of particle size probability; ATP=Arithmetic percentage.

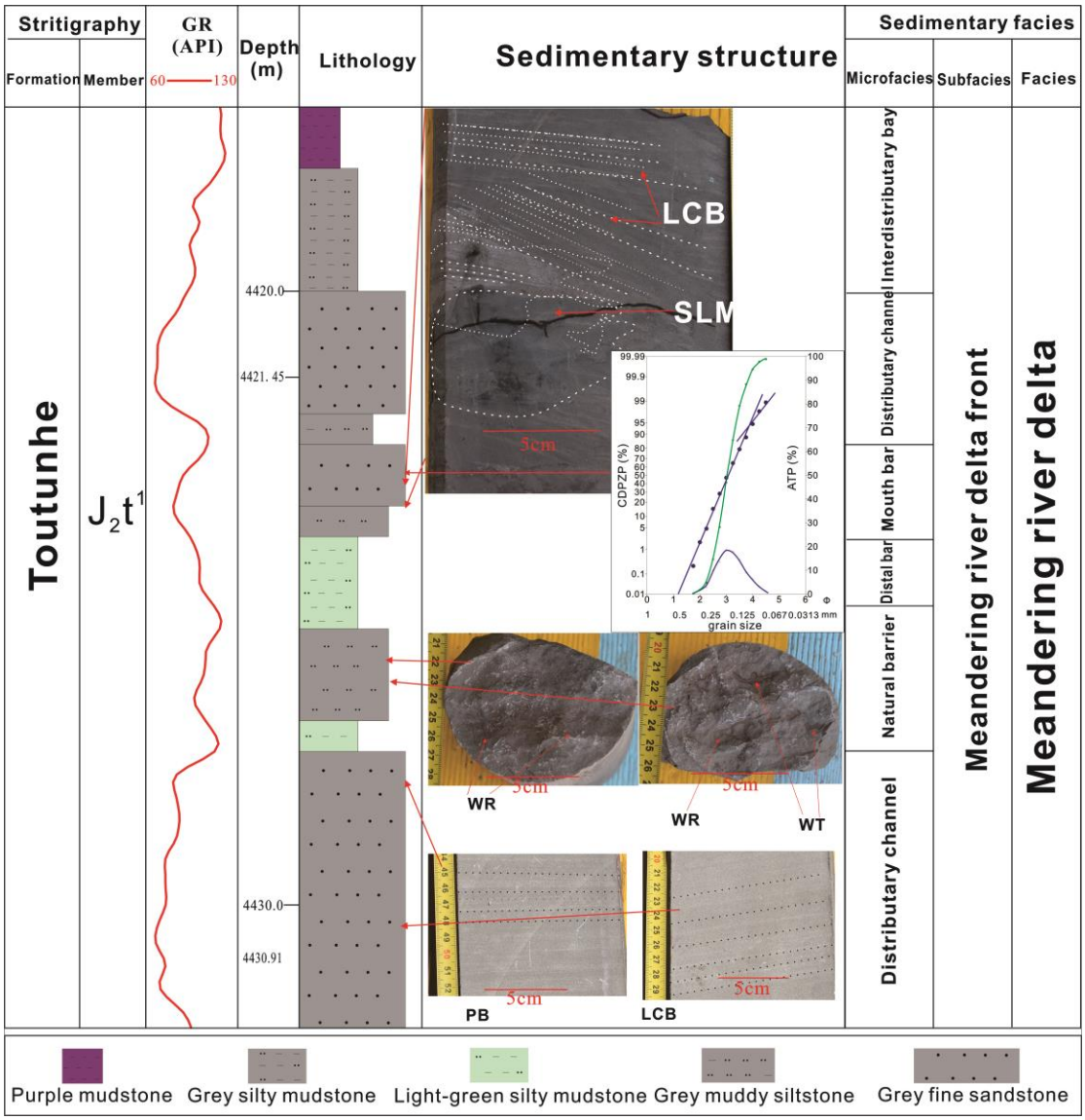

Fig. 12 Lithofacies, logging characteristics, sedimentary structures and sedimentary facies analysis of facies association B. CF= Carbon fragment; PB=Parallel bedding; CB= Current bedding; Lenticular bedding; LCB=Low-angle cross bedding; WR=Wave ripples; WT=Wormtrail; CDPZP=Cumulative distribution of particle size probability; ATP=Arithmetic percentage.

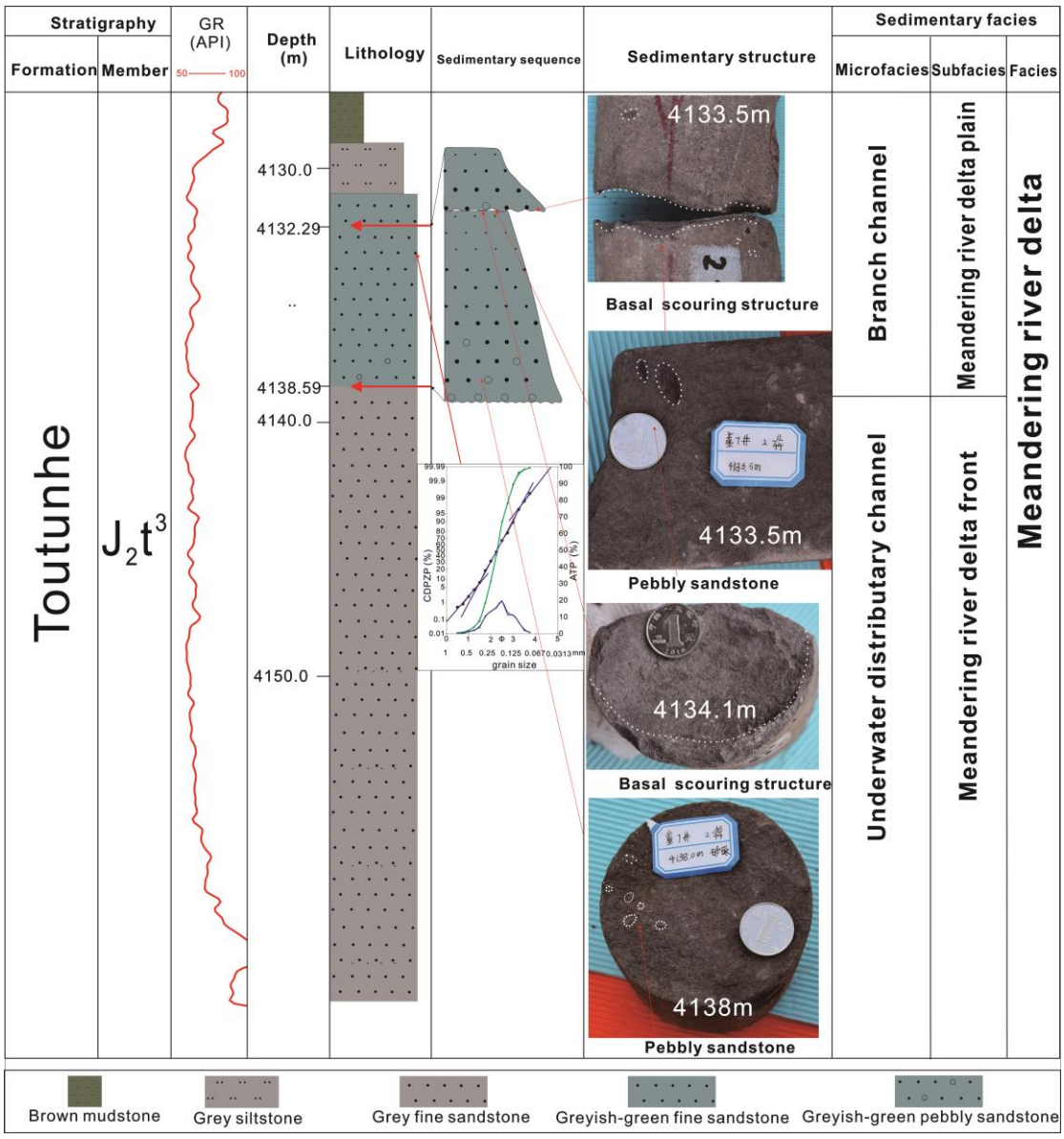

Fig. 13 Lithofacies, logging characteristics, sedimentary structures and sedimentary facies analysis of facies association C. CDPZB=Cumulative distribution of particle size probability; ATP=Arithmetic percentage.

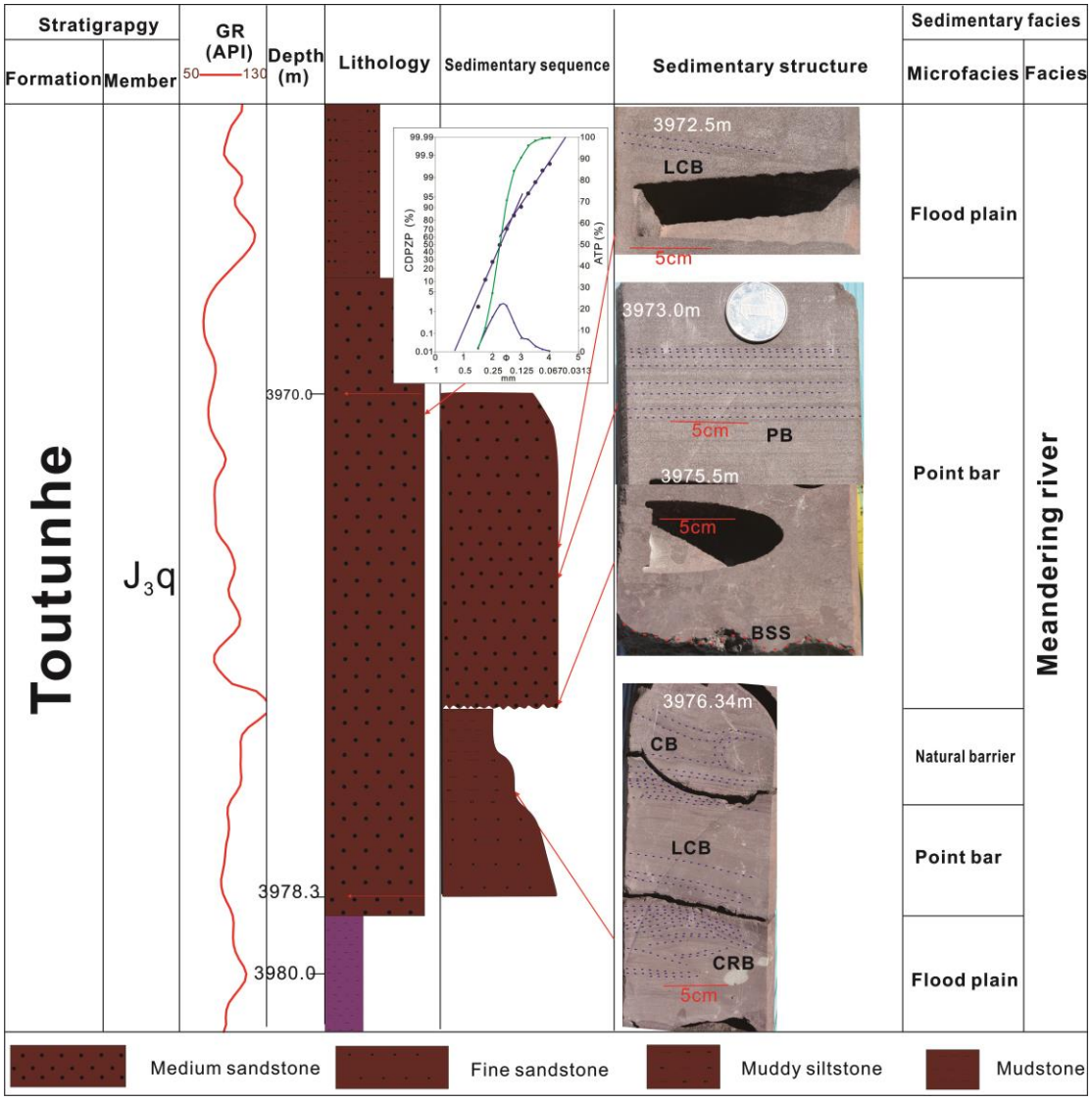

Fig. 14 Lithofacies, logging characteristics, sedimentary structures and sedimentary facies analysis of facies association D. CF= Carbon fragment; PB=Parallel bedding; CB= Current bedding; Lenticular bedding; LCB=Low-angle cross bedding;CRB=Climbing ripple bedding; BSS=Basal scouring structure; CDPZB=Cumulative distribution of particle size probability; ATP=Arithmetic percentage.

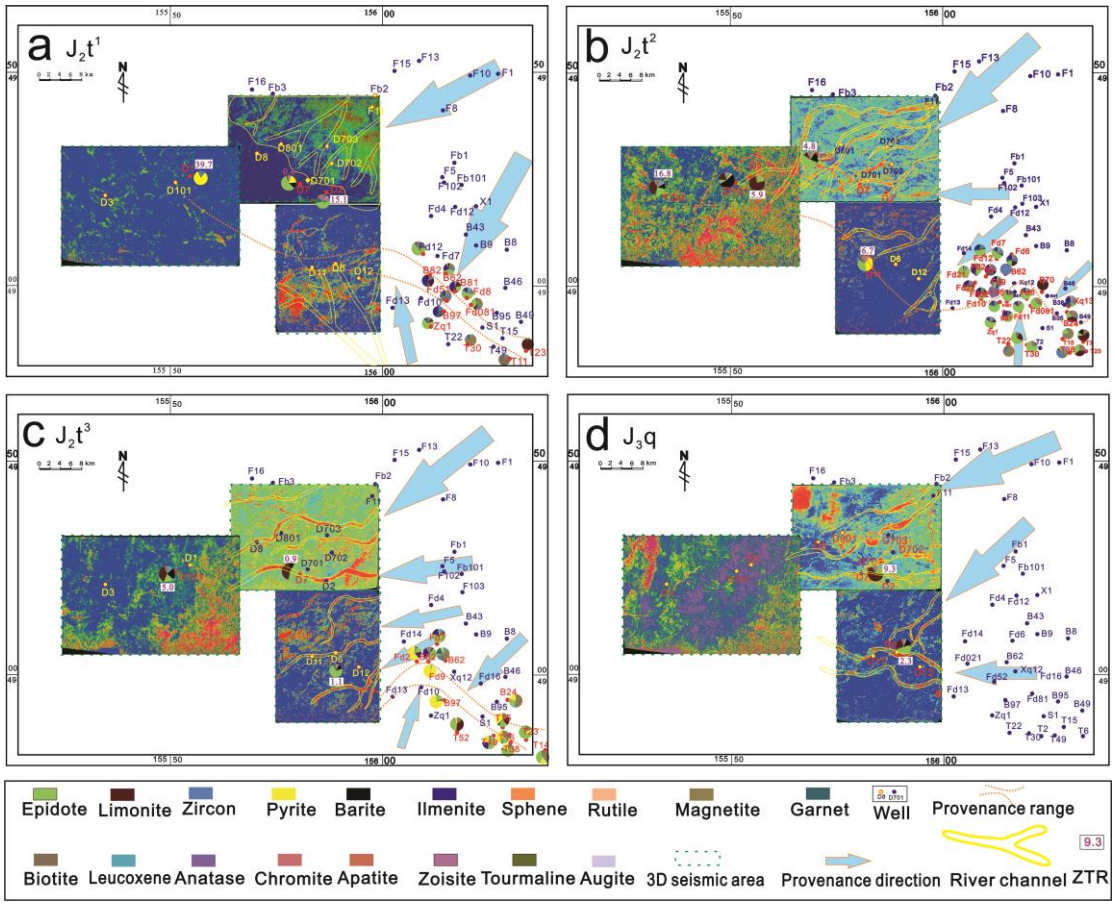

Fig. 15 The heavy mineral distribution, 3D-seismic slices (amplitude attribute), and the analysis of provenance and sedimentary system in the J_2t^1 (A), J_2t^2 (B), J_2t^3 (C) and J_3q (D) (The heavy minerals data in East Fukang slope from Ji et al.,2014). A : 3D-seismic slices showing many channels along northeastern trend and some south sediment source, the distribution (the relative contents of epidote in northeastern and in south Zq1well are higher than the middle) and ZTR (ZTR value increase toward southwest) of heavy minerals northeastern and south provenance; B: 3D-seismic slices showing channels along northeastern and eastern trend, the distribution (the relative contents of epidote decrease toward southwesten in most part of study area and increase toward southern in southeastern part of study area) and ZTR (ZTR value increase toward southwest) of heavy minerals showing main northeastern and eastern provenances and

limited south provenance; C: 3D-seismic slices showing channels along northeastern and eastern trend, the distribution (the relative contents of epidote decrease toward southwesten in most part of study area and increase toward southern in southeastern part of study area) and ZTR (ZTR value increase toward southwest) of heavy minerals showing main northeastern and eastern provenances and limited south provenance; D: 3D-seismic slices showing channels along northeastern trend and east-west trend, the distribution (the relative contents of epidote decrease toward east-west trend) and ZTR (ZTR value increase toward east-west trend) of heavy minerals showing northeastern and eastern provenances;

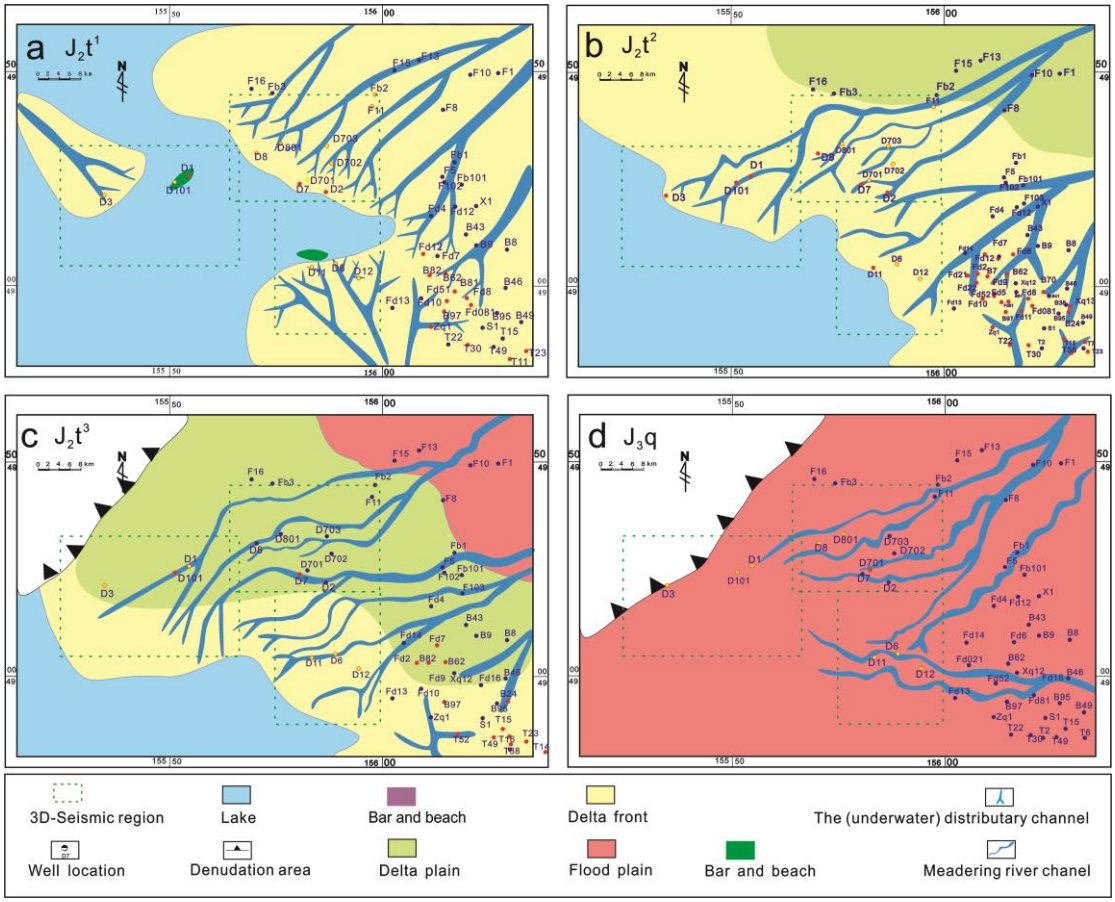

Fig. 16 Distribution characteristics of sedimentary facies in different formations of Shishigou Group in the Centeral-eastern Fukang Sag. A=The sedimentary facies of first member of Toutunhe Formation(J2t1); B= The sedimentary facies of second member of Toutunhe Formation(J2t2); C= The sedimentary facies of third member of Toutunhe Formation(J2t3); The sedimentary facies of Qigu Formation(J3q);

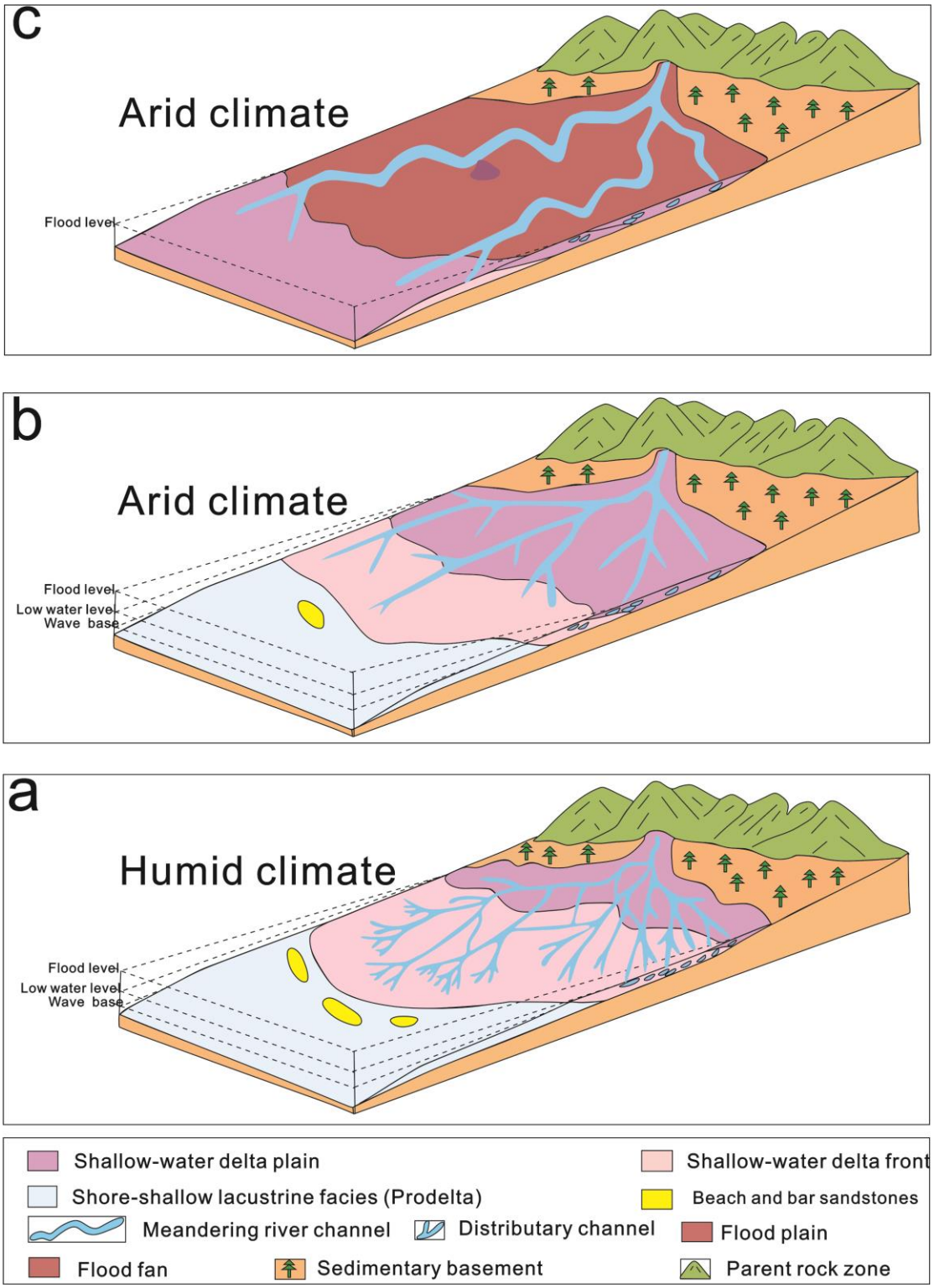

Fig. 17 Sedimentary model for the lake-shallow water delta-meandering river sedimentary system in different climate conditions. Modified from Zhu et al., 2012.

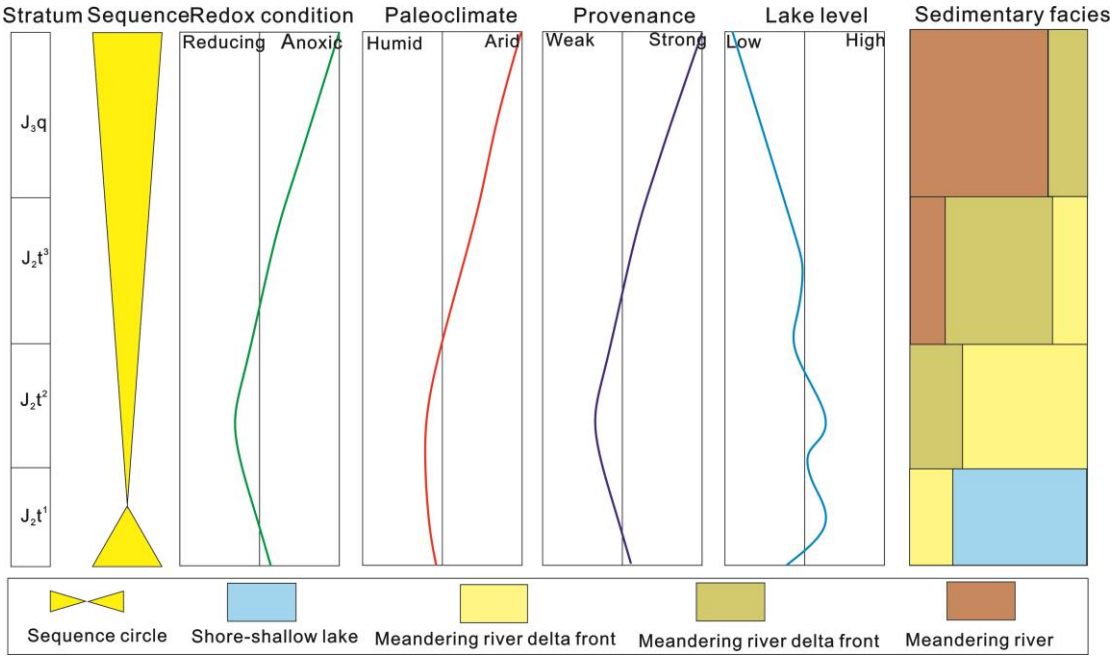

Fig. 18 The relationship between the palaeo-environment, provenance, lake level and sedimentary facies during deposition of the Middle-Late Jurassic Shishugou Group in the Central Juggar Basin. Lake level curve was modified from the Zhu et al. (2017).